Electronic Supplementary Material (ESI) for Chemical Science.
This journal is © The Royal Society of Chemistry 2021

Supporting information for

Polarization-Induced Charge Separation in Conjugated Microporous Polymers for Efficient Visible Light-Driven C-3 Selenocyanation of Indoles

Qiujian Xie,[a] Yumin Yang,[b] Weijie Zhang,[a] Zhu Gao,[a] Xiaofeng Li,[a] Juntao Tang,*[a] Chunyue Pan,[a] Guipeng Yu*[a]

*Corresponding author:

Guipeng Yu (E-mail: gilbertyu@csu.edu.cn)

Juntao Tang (E-mail: reynardtang@csu.edu.cn)

Postal address:

[†] Hunan Key Laboratory of Micro & Nano Materials Interface Science, College of Chemistry and Chemical Engineering, Central South University, LushanSouth Road 932, Changsha 410083, Hunan, P. R. China;

[‡]Queen Mary University of London Engineering School, Northwestern Polytechnical University, YouyiWest Road 127, Xian 710072, Shaanxi, P. R. China.

Table of Contents

1. Characterizations ····· **S-3**

2. Synthesis of Monomers ····· **S-4**

3. Photocatalyst Characterizations ····· **S-6**

4. Density Functional Calculation Information ····· **S-17**

5. NMR Spectra of Monomers and Products ····· **S-22**

6. Supplementary References ····· **S-39**

1. Characterizations

^{1}H and ^{13}C NMR spectra were measured with the deuterated solvents ($CDCl_3$ and DMSO-d6) and employed the tetramethyl silane (TMS) as an internal standard (Bruker AM-400 MHz NMR spectrometer). The obtained samples were prepared by dispersing in KBr powder and the corresponding FT-IR spectra were measured in the 4000-400 cm^{-1} region (VARIAN 1000 FT-IR spectrometer). The solid-state ^{13}C/NMR spectra of the polymers were carried out by using an Avance III HD 400 NMR spectrometer. Surface areas were measured by nitrogen adsorption and desorption at 77 K using Micromeritics ASAP 2020M. The pore-size-distribution of the polymers were acquired by the adsorption branches (non-local density functional theory method, NLDFT). The polymers surface morphologies were carried out at an accelerating voltage of 8.0 kV (FEI SIRION200). The UV-Vis adsorption spectra of the powders in the solid state were obtained on a scan UV-Vis spectrophotometer (U-4100 spectrometer). The electrochemical impedance spectra (EIS) was performed on an electrochemical workstation at room temperature in the dark (CHI760E). The photocurrent of the polymer was performed on a VersaSTAT 3 electrochemical workstation under irradiation of 300 W Xe lamp. The fluorescence spectra were characterized by using excitation wavelength of 365 nm at room temperature (F97PRO fluorescence spectrometer). The time-correlated fluorescence spectroscopy of solid samples was performed on a FLS-980 fluorescence lifetime spectrometer. The cyclic voltammetry (CV) measurements were carried out on an electrochemical workstation system in a 0.1 M Bu_4NPF_6 solution (0.1 V/s, CHI660E). The density functional theory (DFT) calculations was applied to optimize the geometry of monomers and oligomers (B3LYP functional, and 6-31G(d) basis set). The time-dependent density functional theory (TD-DFT) was utilized to calculated electronic transitions of the monomers (CAM-B3LYP functional, and 6-31G(d) basis set). The molecular configuration optimization and electrostatic potential map was carried out by DFT calculations (Gaussian 09 software package and Gauss View visualization program). The transition density matrix (TDM) heat map of electron and hole contribution of excited monomer fragments were constructed by the Multiwfn 3.6 program. The optimal configuration and natural dipole moment of monomers are visualized by the VMD 1.9.3 program.

2. Synthesis and Characterization of Monomers and Polymers

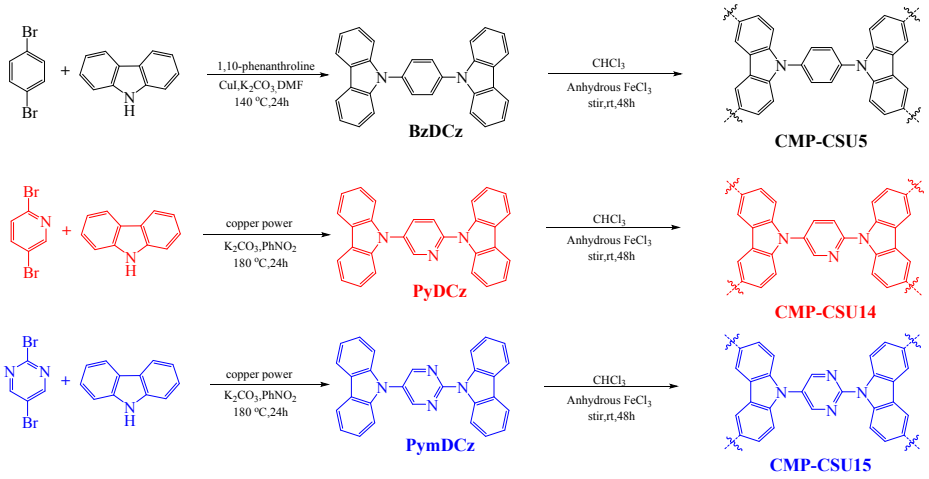

Scheme 1. The synthetic route of monomers and polymers.

Synthesis of 9,9'-(benzene)-bis(9H-carbazole) (BzDCz)

A mixture of 1,4-dibromobenzene (3 g, 10.6 mmol), potassium carbonate (5.3 g, 38.2mmol), copper iodide (200 mg, 1.1 mmol), 1,10-phenanthroline (190 mg, 1.1 mmol), carbazole (6.4 g, 38.2 mmol) in dry N, N-dimethylformamide (80 mL) was stirred for 24 hours at 140 °C under N_2. After cooling to room temperature, the reaction mixture was concentrated to remove the solvent. The residue was purified by flash column chromatography to remove the byproduct, and the resulting mixture was suspended in dichloromethane (20 mL) and stirred for one hour. The filtrate was concentrated and performed for two times following the above steps. The desired product was obtained as a white solid in 66 % yield. ^{1}H NMR (400 MHz, $CDCl_3$): δ 8.23-8.21 (d, 4H), 7.84 (s, 4H), 7.61-7.59 (d, 4H), 7.53-7.50 (t, 4H), 7.39-7.36 (t, 3H). ^{13}C NMR (100 MHz, $CDCl_3$): δ 140.79, 136.70, 128.40, 126.16, 123.60, 120.48, 120.31, 109.78.

Synthesis of 9, 9'-(Pyridine-2, 5-diyl) bis(9H-carbazole) (PyDCz)[1]

The mixture of 2,5-dibromopyridine (3 g, 12.8 mmol), 9H-carbazole (6.5 g, 38.9 mmol), copper power (1.12 g, 11.3 mmol) and potassium carbonate (15.7 g, 113 mmol) in 40 mL nitrobenzene was stirred for 48 hours at 180 °C. After cooling to room temperature, the reaction mixture was extracted with dichloromethane for three times (3×50 mL). The organic phase was separated and concentrated under reduced pressure. The crude solid product was further purified by column chromatography on silica gel with PE/DCM (v/v = 2/1) as the eluent to afford a white solid in 90% yield. ^{1}H NMR (400 MHz, $CDCl_3$): δ 8.99 (d, J = 2.6 Hz, 1H), 8.32–8.10 (m, 5H), 8.03 (d, J = 8.3 Hz, 2H), 7.92 (d, J = 8.5 Hz, 1H), 7.61–7.44 (m, 6H), 7.44–7.33 (m, 4H). ^{13}C NMR (100 MHz, $CDCl_3$, ppm): δ 150.55, 148.01, 140.73, 139.45, 136.84, 131.83, 126.43, 126.40, 124.59, 123.79, 121.38, 120.72, 120.62, 120.35, 119.35, 111.34, 109.39.

Synthesis of 9, 9'-(Pyrimidine-2, 5-diyl) bis(9H-carbazole) (PymDCz)

PymDCz (yield: 85%) was prepared under the identical synthetic conditions described in the preparation of PyDCz using 2,5-dibromopyrimidine (3 g, 12.7 mmol), 9H-carbazole (6.5 g, 38.9 mmol), copper power (1.12 g, 11.3 mmol) and potassium carbonate (15.7 g, 113 mmol). ^{1}H NMR (400 MHz, $CDCl_3$, ppm): δ 9.08 (s, 2H), 8.99 (d, J = 8.4 Hz, 2H), 8.20 (d, J = 7.8 Hz, 2H), 8.12 (d, J = 7.1 Hz, 2H), 7.61–

7.34 (m, 10H). ^{13}C NMR (100 MHz, $CDCl_3$): δ 157.61, 156.48, 140.81, 139.14, 127.77, 126.87, 126.55, 126.12, 123.86, 122.83, 120.94, 120.72, 119.67, 116.64, 109.13.

Recycle experiments based on CMP-CSU14

1-*H* Indole (0.2 mmol), KSeCN (0.4 mmol, 2 equiv), tetrahydrofuran (2 mL) and CMP-CSU14 (10 mg) were transferred to a transparent reaction tube. The reaction mixture was degassed and protected with an O_2 balloon (~0.1 MPa) and then stirred under irradiation with the light source (a 14 W blue LED, 0.20 W/cm^2, distance app.8 cm) for 24 hours. After each cycle was completed, the photocatalyst (CMP-CSU14) was gathered by centrifugation, washed with tetrahydrofuran and water repeatedly to remove products and unreacted substrates, dried at 100 °C in vacuum for 12 hours. After that, the collected CMP-CSU14 was re-applied for next cycle.

3. Photocatalyst Characterizations

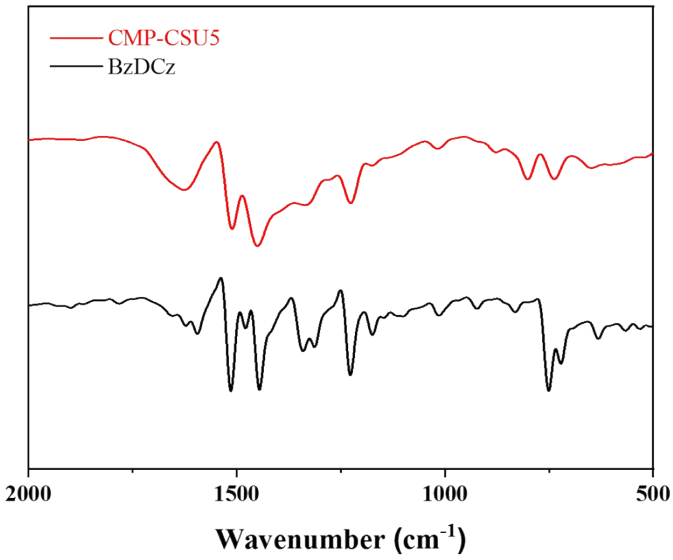

Fig. S1 Partial FT-IR spectra of BzDCz and CMP-CSU5.

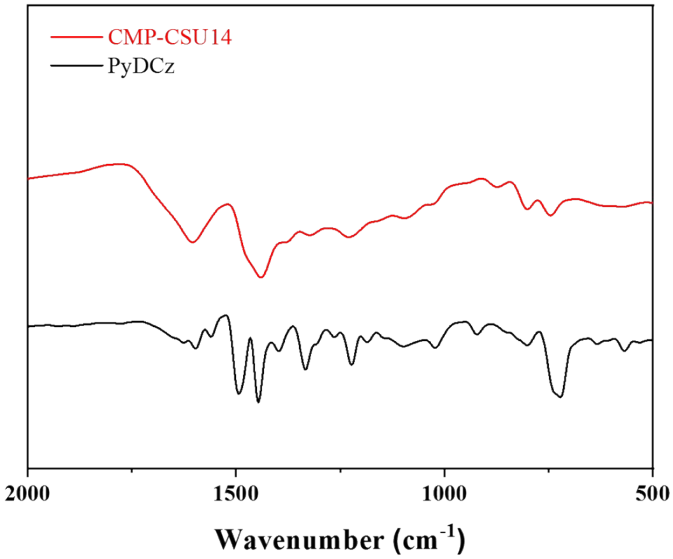

Fig. S2 Partial FT-IR spectra of PyDCz and CMP-CSU14.

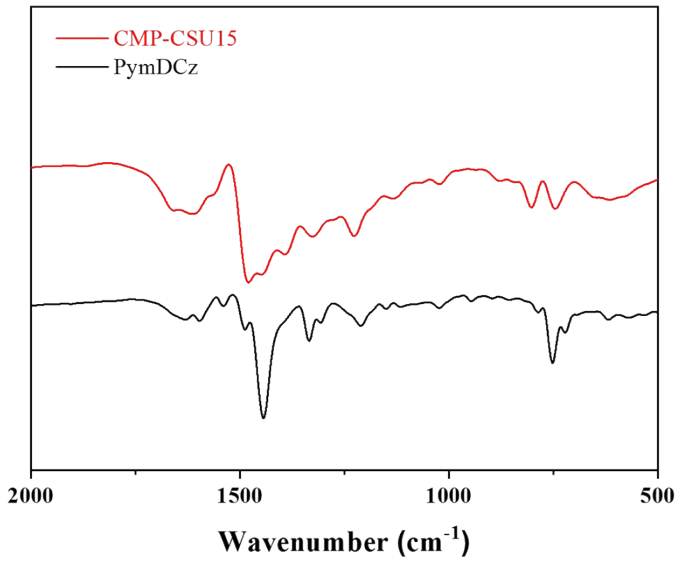

Fig. S3 Partial FT-IR spectra of PymDCz and CMP-CSU15.

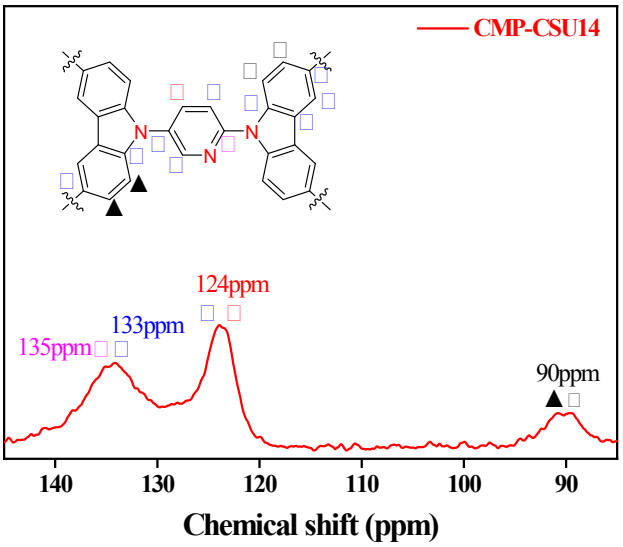

Fig. S4 Solid-state ^{13}C CP-MAS NMR spectrum of CMP-CSU14.

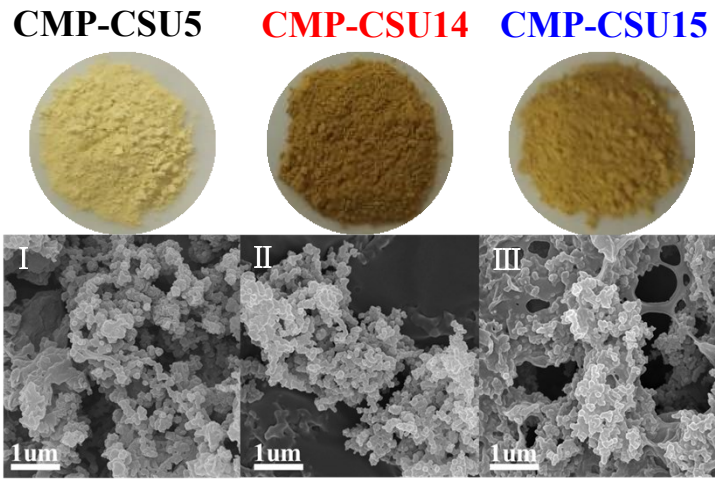

Fig. S5 Photograph and scanning electron microscopy (SEM) image of (I) CMP-CSU5, (II) CMP-CSU14, and (III) CMP-CSU15.

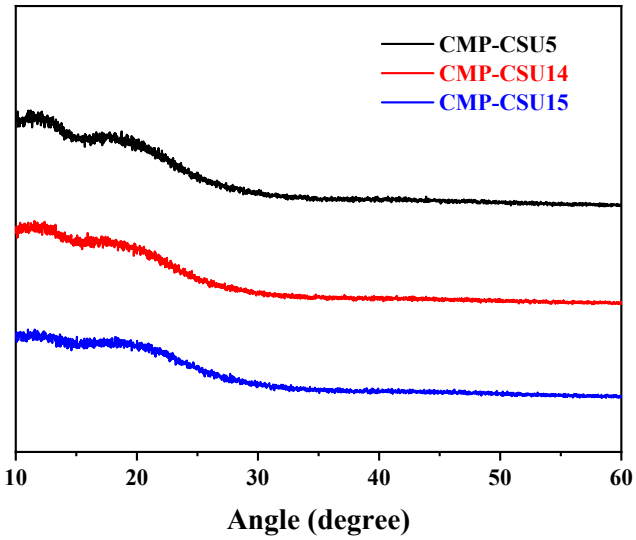

Fig. S6 Powder XRD analysis of CMP-CSU5, CMP-CSU14, and CMP-CSU15.

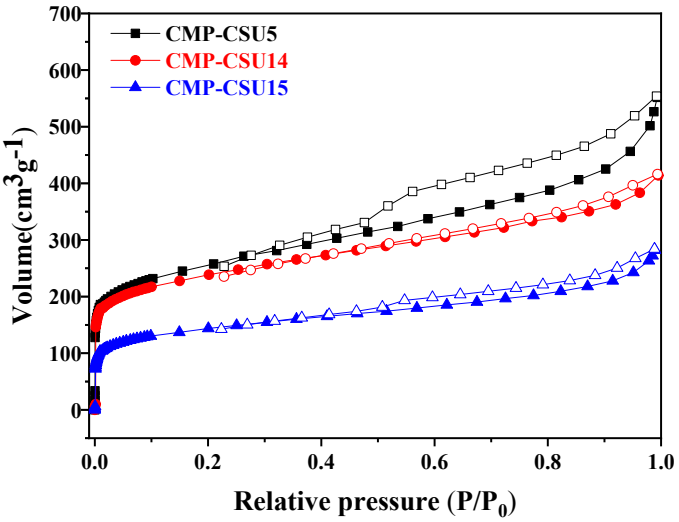

Fig. S7 Nitrogen adsorption (solid circle) and desorption (open circle) isotherm of CMP-CSU5, CMP-CSU14 and CMP-CSU15 at 77 K.

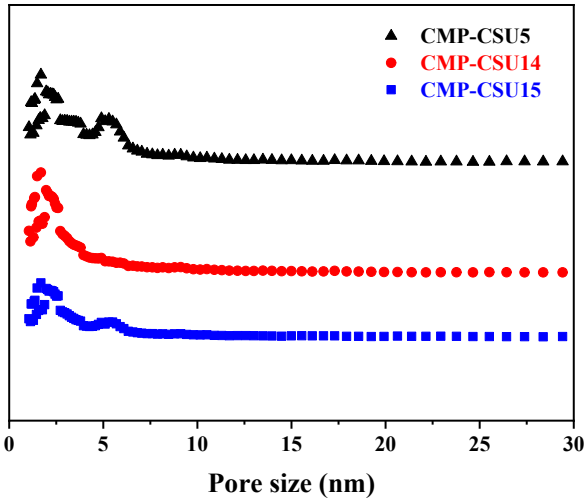

Fig. S8 Pore size distribution of CMP-CSU5, CMP-CSU14, CMP-CSU15.

Table S1. Porosity data of CMP-CSU5, CMP-CSU14, CMP-CSU15.

Samples	S_{BET} ($m^2\ g^{-1}$)	V_{total} ($cm^3\ g^{-1}$)	V_{meso}/V_{total} (%)
CMP-CSU5	912.3	0.79	87%
CMP-CSU14	867.3	0.59	71%
CMP-CSU15	528.6	0.39	75%

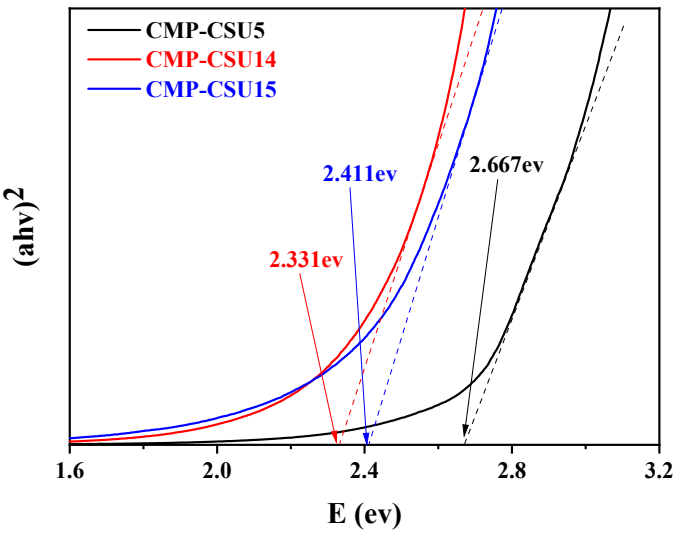

Fig. S9 Tauc plots of the transformed Kubelka-Munk function of CMP-CSUs.

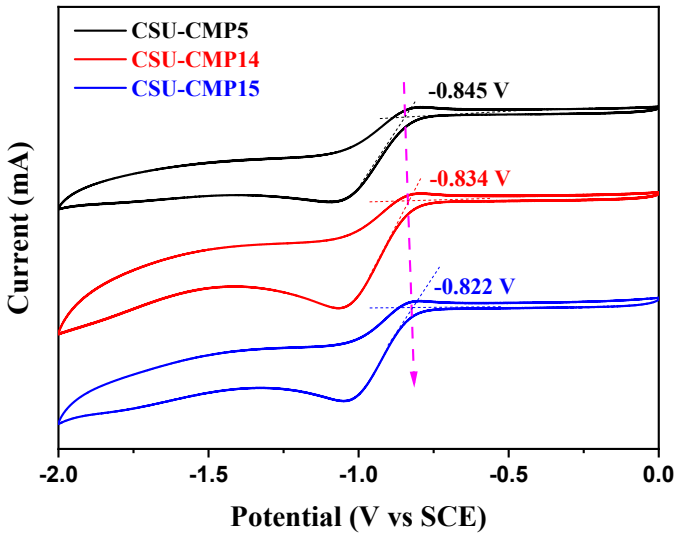

Fig. S10 Cyclic voltammetry curves of CMP-CSUs in deaerated CH_3CN with 0.1 M Bu_4PF_6 as supporting electrolyte with scan rate of 0.1 V/s.

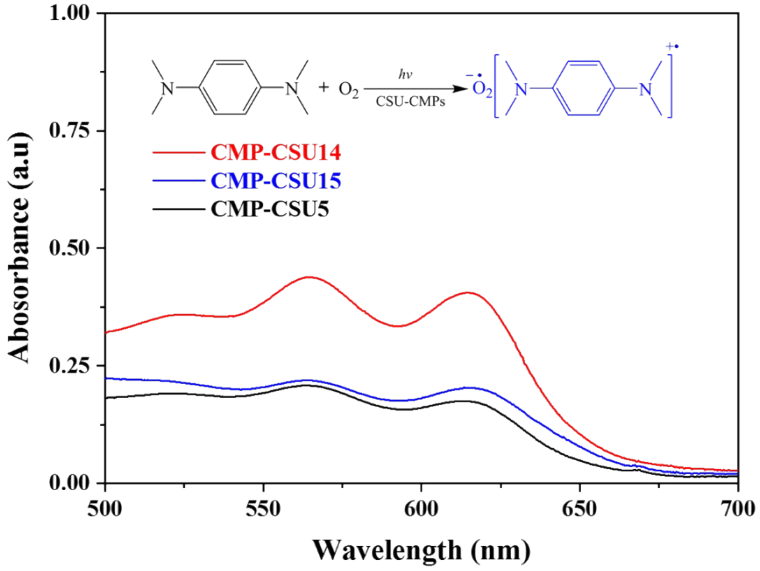

Fig. S11 UV-vis absorption spectra and photograph of the cationic radical of TMPD generated by CMP-CSUs in the presence of light and oxygen.

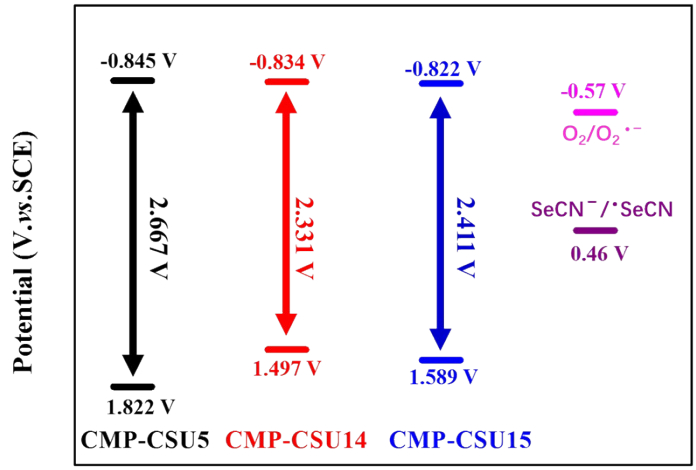

Fig. S12 LUMO and HOMO positions of CMP-CSUs.

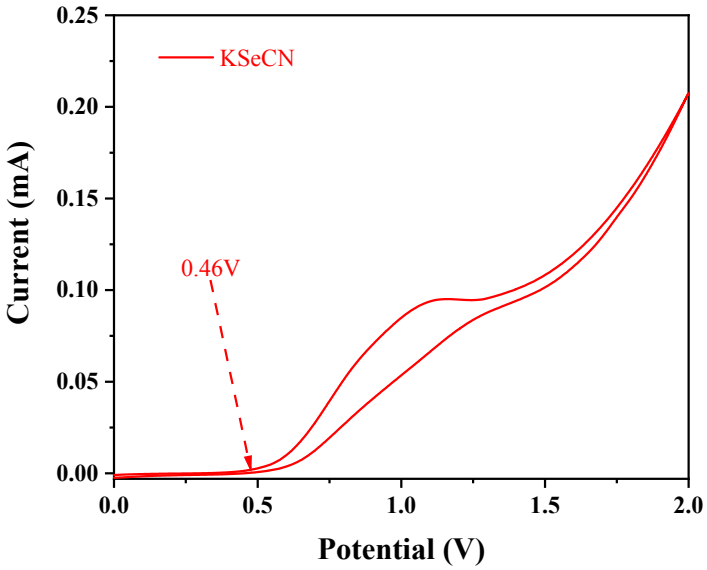

Fig. S13 Cyclic voltammetry of potassium selenocyanate (KSeCN) with a scan rate of 0.01 V/s.

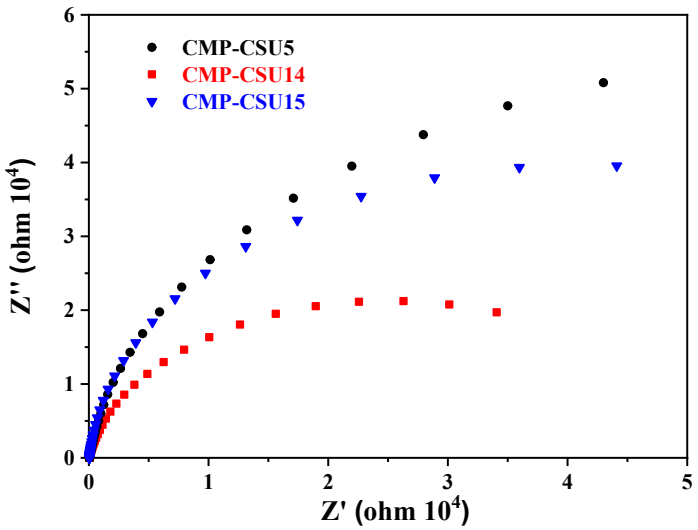

Fig. S14 Electrochemical impedance spectroscopy (EIS) Nyquist plots of CMP-CSUs.

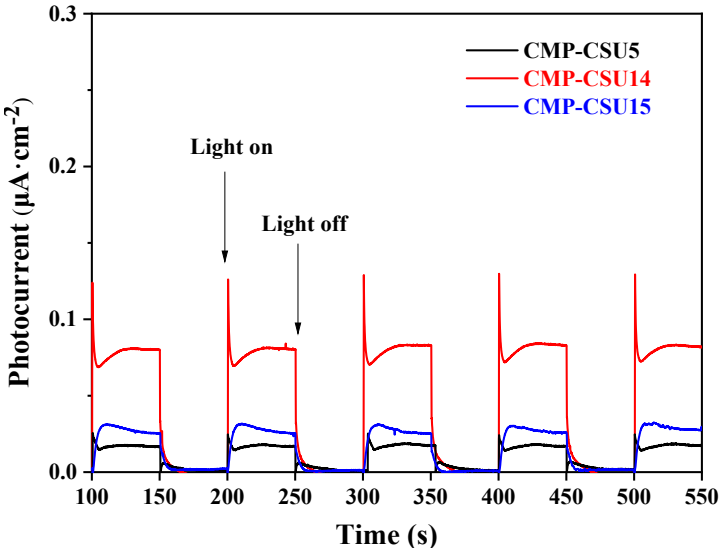

Fig. S15 Transient photocurrent of CMP-CSUs.

Table S2. Fitted decay time of CMP-CSUs.

Photocatalyst	τ_1 (ns)	τ_2 (ns)	average time (ns)
CMP-CSU5	0.50	2.11	0.70
CMP-CSU14	0.55	4.76	2.56
CMP-CSU15	0.39	3.95	2.46

τ_1 can be attributed to the radiative recombination of the photogenerated charge carriers, and the τ_2 mainly represent the lifetimes of nonradiative and energy transfer process; A_1 and A_2 are the pre-exponential factors of decay curves.

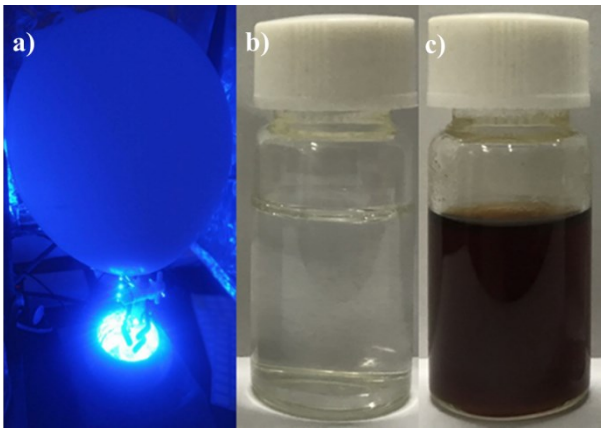

Fig. S16 (a) Photograph of C-3 Selenocyanation of indoles based on CMP-CSU14 under UV light; photograph of reaction mixture (b) before reaction (c) after reaction under UV light for 24 hours.

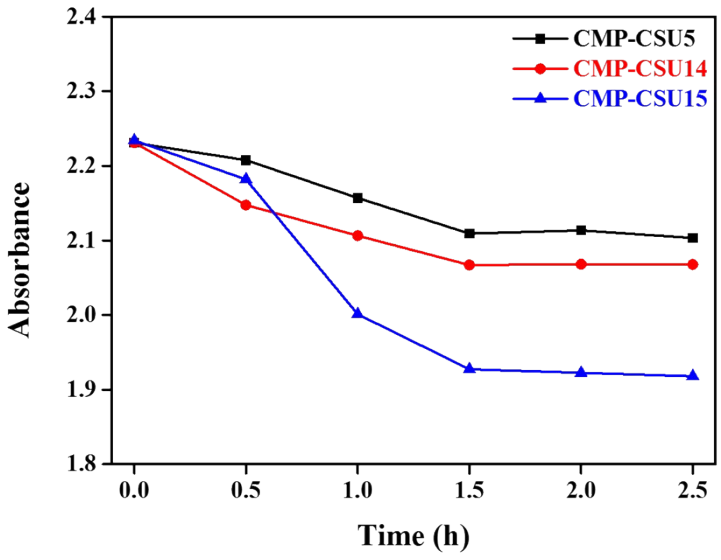

Fig. S17 Adsorption behavior of CMP-CSUs towards 1-H Indole in dark condition.

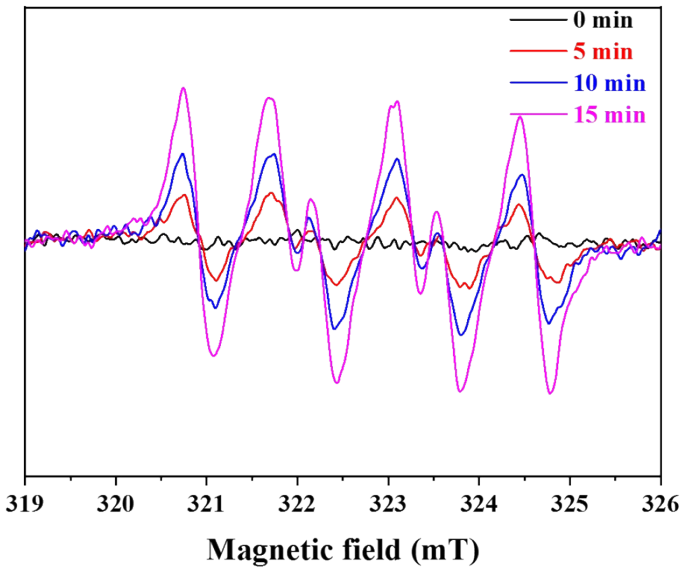

Fig. S18 EPR spectra of a mixture of CMP-CSU14 and DMPO upon light irradiation for 15 minutes (pink line), 10 minutes (blue line), 5 minutes (red line) and 0 minutes in the dark (black line).

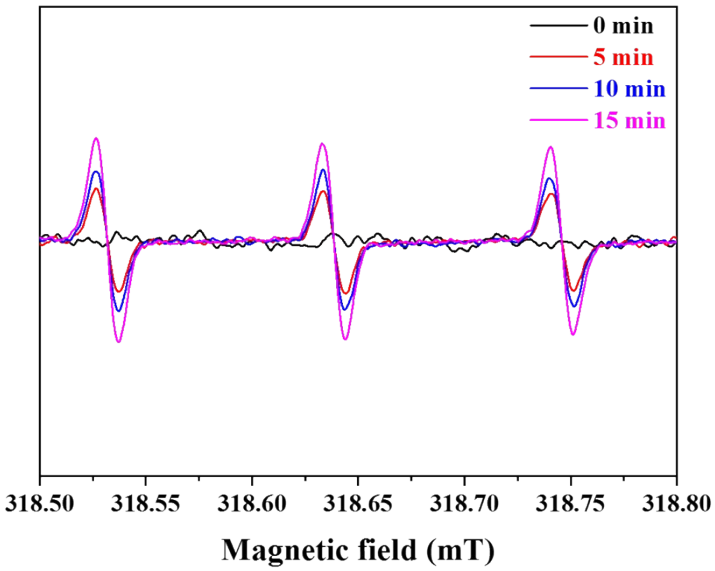

Fig. S19 EPR spectra of a mixture of CMP-CSU14 and TEMP upon light irradiation for 15 minutes (pink line), 10 minutes (blue line), 5 minutes (red line) and 0 minutes in the dark (black line).

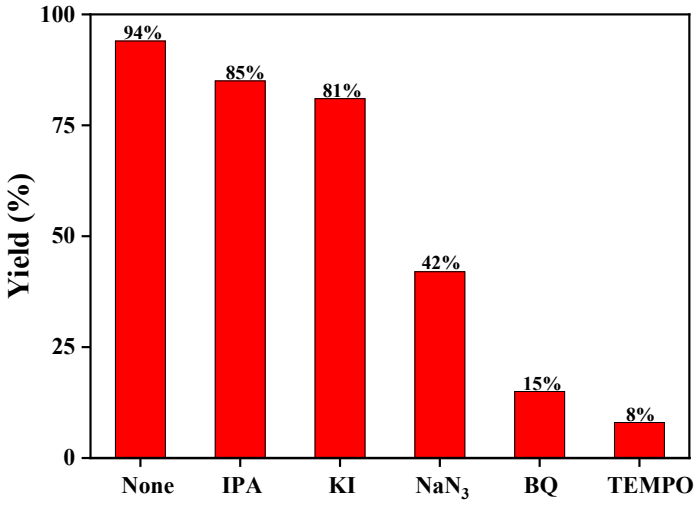

Fig. S20 Control experiments for the C-3 selenocyanation of indoles.

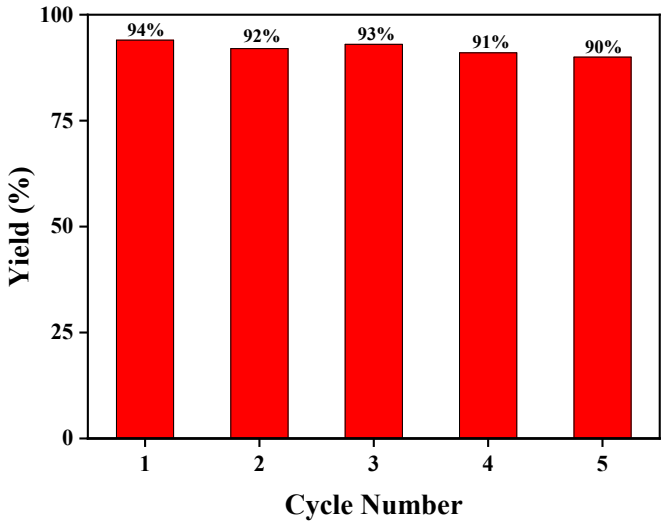

Fig. S21 Recycled performance of the CMP-CSU14 for the C-3 selenocyanation of indoles.

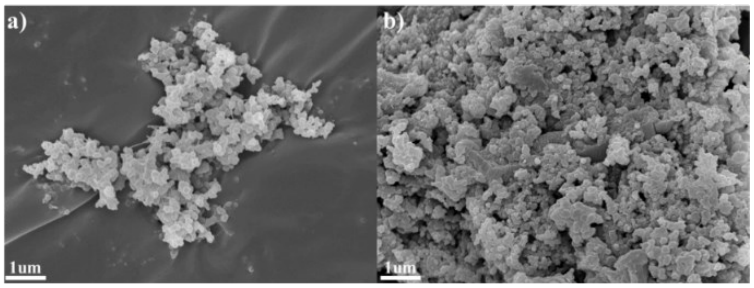

Fig. S22 Scanning electron microscopy (SEM) images of CMP-CSU14 (a)before and (b)after five runs under UV-Visible light.

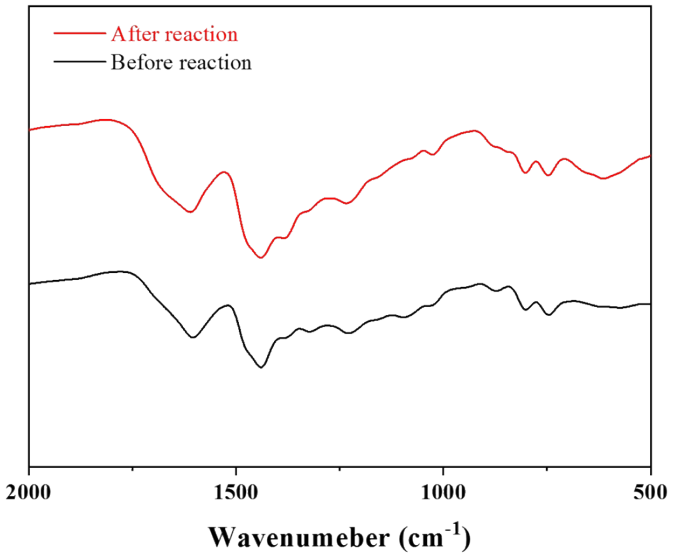

Fig. S23 Partial FT-IR spectra for CMP-CSU14 before and after reused five times under UV-Visible light.

Table S3. Optimization of Reaction Conditions for C-3 Selenocyanation of 1*H*-Indole [a].

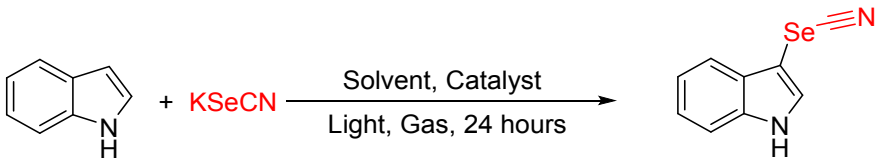

Entry	Solvent	Light	O_2/N_2	Yield[b] (%)
1	THF	+	O_2	94
2	MeCN	+	O_2	54
3	DCM	+	O_2	21
4	MeOH	+	O_2	23
5	DMF	+	O_2	12
6[c]	THF	-	O_2	Trace
7[d]	THF	+	N_2	18
8[e]	THF	+	O_2	55

[a]Reaction conditions: 1-*H* indole (0.2 mmol), KSeCN (0.4 mmol, 2.0 equiv), CMP-CSU14 (10 mg), tetrahydrofuran (THF 2 mL), RT = 25 ± 2 °C, 24 h, O_2 (~0.1 MPa), using a 14 W LED lamp (0.20 W/cm^2) as the light source. [b] ^{1}HNMR yield (using mesitylene as an internal standard). [c] No Light. [d] O_2 was replaced by N_2. [e] 1.0 equiv of KSeCN was used.

4. DFT Calculation Information

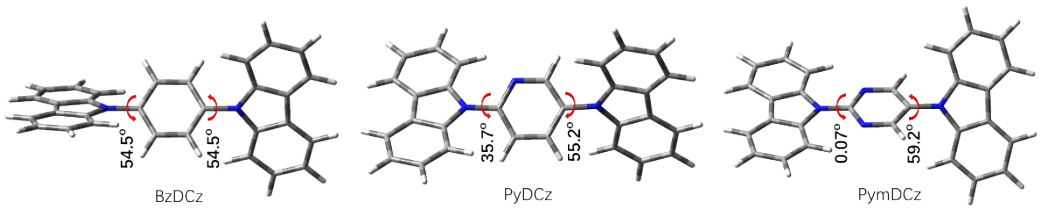

Fig. S24 Dihedral angles of monomers from DFT geometry optimizations.

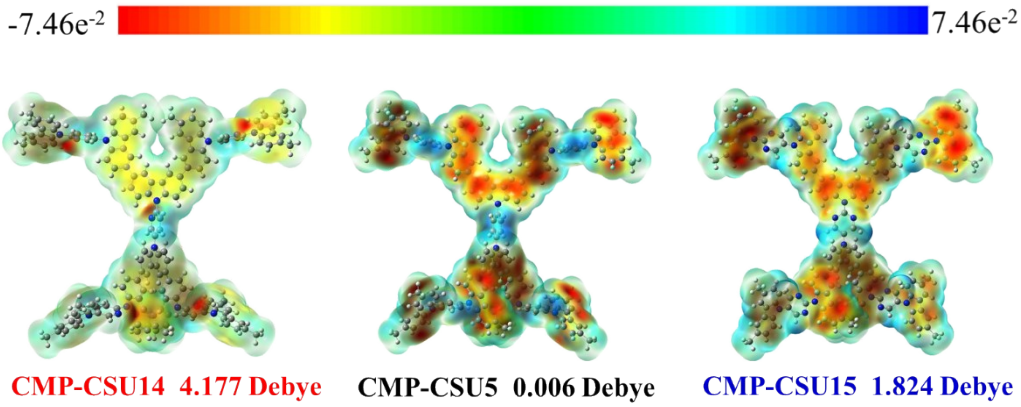

Fig. S25 Diagram of molecular dipoles for the oligomers of CSU-CMPs (unit of dipole moment: Debye).

Table S4. The first excited state index of the monomer.

Sample	D_c	S_r	H	t	E_{s1}	Dipole
BzDCz	0.01	0.828	0.431	-4.428	4.386ev	0.0005D
PyDCz	0.546	0.613	3.421	-2.255	4.098ev	1.90661D
PymDCz	0.835	0.523	2.671	-1.201	3.967ev	1.0861D

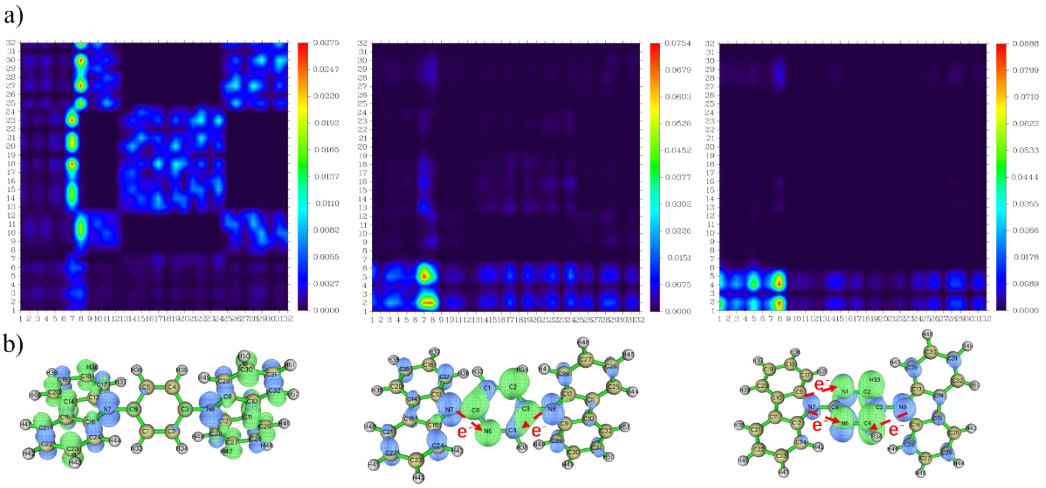

Fig. S26 (a) Transition density matrix heat map of electrons and holes distribution of the excited monomer atoms, (b) Holes and electrons distribution of excited monomers (green represent electron; blue represent Hole) [2].

Table S5. The holes and electrons contribution of BzDCz atoms by the multifunctional wavefunction analyzer.

The number of non-hydrogen atoms: 32

Contribution of each non-hydrogen atom to hole and electron:

1(C)	Hole:	1.05 %	Electron:	0.62 %	Overlap:	0.80 %	Diff.:	-0.43 %
2(C)	Hole:	1.05 %	Electron:	0.61 %	Overlap:	0.80 %	Diff.:	-0.44 %
3(C)	Hole:	1.32 %	Electron:	1.84 %	Overlap:	1.56 %	Diff.:	0.52 %
4(C)	Hole:	1.05 %	Electron:	0.61 %	Overlap:	0.80 %	Diff.:	-0.44 %
5(C)	Hole:	1.05 %	Electron:	0.62 %	Overlap:	0.80 %	Diff.:	-0.43 %
6(C)	Hole:	1.32 %	Electron:	1.85 %	Overlap:	1.57 %	Diff.:	0.53 %
7(N)	Hole:	11.18 %	Electron:	0.60 %	Overlap:	2.59 %	Diff.:	-10.58 %
8(N)	Hole:	11.20 %	Electron:	0.60 %	Overlap:	2.59 %	Diff.:	-10.60 %
9(C)	Hole:	1.51 %	Electron:	2.36 %	Overlap:	1.89 %	Diff.:	0.85 %
10(C)	Hole:	2.98 %	Electron:	4.39 %	Overlap:	3.62 %	Diff.:	1.42 %
11(C)	Hole:	2.98 %	Electron:	4.39 %	Overlap:	3.62 %	Diff.:	1.42 %
12(C)	Hole:	1.51 %	Electron:	2.36 %	Overlap:	1.89 %	Diff.:	0.85 %
13(C)	Hole:	1.51 %	Electron:	2.36 %	Overlap:	1.89 %	Diff.:	0.86 %
14(C)	Hole:	2.97 %	Electron:	4.39 %	Overlap:	3.61 %	Diff.:	1.42 %
15(C)	Hole:	2.97 %	Electron:	4.39 %	Overlap:	3.61 %	Diff.:	1.42 %
16(C)	Hole:	1.51 %	Electron:	2.36 %	Overlap:	1.89 %	Diff.:	0.86 %
17(C)	Hole:	4.64 %	Electron:	3.21 %	Overlap:	3.86 %	Diff.:	-1.43 %
18(C)	Hole:	0.96 %	Electron:	6.53 %	Overlap:	2.50 %	Diff.:	5.57 %
19(C)	Hole:	5.17 %	Electron:	1.09 %	Overlap:	2.38 %	Diff.:	-4.07 %
20(C)	Hole:	2.42 %	Electron:	5.49 %	Overlap:	3.64 %	Diff.:	3.07 %
21(C)	Hole:	2.42 %	Electron:	5.49 %	Overlap:	3.64 %	Diff.:	3.07 %
22(C)	Hole:	5.17 %	Electron:	1.09 %	Overlap:	2.38 %	Diff.:	-4.07 %
23(C)	Hole:	0.96 %	Electron:	6.53 %	Overlap:	2.50 %	Diff.:	5.57 %
24(C)	Hole:	4.64 %	Electron:	3.21 %	Overlap:	3.86 %	Diff.:	-1.43 %
25(C)	Hole:	2.42 %	Electron:	5.51 %	Overlap:	3.65 %	Diff.:	3.09 %
26(C)	Hole:	5.17 %	Electron:	1.09 %	Overlap:	2.38 %	Diff.:	-4.08 %
27(C)	Hole:	0.96 %	Electron:	6.54 %	Overlap:	2.50 %	Diff.:	5.58 %
28(C)	Hole:	4.65 %	Electron:	3.22 %	Overlap:	3.87 %	Diff.:	-1.43 %
29(C)	Hole:	4.65 %	Electron:	3.22 %	Overlap:	3.87 %	Diff.:	-1.43 %
30(C)	Hole:	0.96 %	Electron:	6.54 %	Overlap:	2.50 %	Diff.:	5.58 %
31(C)	Hole:	5.17 %	Electron:	1.09 %	Overlap:	2.38 %	Diff.:	-4.08 %
32(C)	Hole:	2.42 %	Electron:	5.51 %	Overlap:	3.65 %	Diff.:	3.09 %

Sum of hole shown above: 99.91% Sum of electron shown above: 99.72%

Table S6. The holes and electrons contribution of PyDCz atoms by the multifunctional wavefunction analyzer.

The number of non-hydrogen atoms: 32

Contribution of each non-hydrogen atom to hole and electron:

1(C)	Hole:	5.48 %	Electron:	2.80 %	Overlap:	3.92 %	Diff.:	-2.68 %
2(C)	Hole:	1.10 %	Electron:	27.61 %	Overlap:	5.51 %	Diff.:	26.51 %
3(C)	Hole:	5.79 %	Electron:	10.99 %	Overlap:	7.98 %	Diff.:	5.20 %
4(C)	Hole:	5.11 %	Electron:	4.74 %	Overlap:	4.92 %	Diff.:	-0.37 %
5(N)	Hole:	1.69 %	Electron:	22.04 %	Overlap:	6.10 %	Diff.:	20.35 %
6(C)	Hole:	3.74 %	Electron:	15.78 %	Overlap:	7.68 %	Diff.:	12.04 %
7(N)	Hole:	15.51 %	Electron:	0.47 %	Overlap:	2.71 %	Diff.:	-15.04 %
8(N)	Hole:	10.65 %	Electron:	0.25 %	Overlap:	1.62 %	Diff.:	-10.41 %
9(C)	Hole:	0.40 %	Electron:	0.78 %	Overlap:	0.56 %	Diff.:	0.38 %
10(C)	Hole:	1.81 %	Electron:	0.53 %	Overlap:	0.98 %	Diff.:	-1.28 %
11(C)	Hole:	1.76 %	Electron:	0.51 %	Overlap:	0.95 %	Diff.:	-1.25 %
12(C)	Hole:	0.42 %	Electron:	1.03 %	Overlap:	0.66 %	Diff.:	0.62 %
13(C)	Hole:	0.66 %	Electron:	1.63 %	Overlap:	1.04 %	Diff.:	0.97 %
14(C)	Hole:	2.62 %	Electron:	1.05 %	Overlap:	1.66 %	Diff.:	-1.57 %
15(C)	Hole:	2.47 %	Electron:	1.08 %	Overlap:	1.64 %	Diff.:	-1.39 %
16(C)	Hole:	0.96 %	Electron:	1.66 %	Overlap:	1.26 %	Diff.:	0.70 %
17(C)	Hole:	5.22 %	Electron:	0.43 %	Overlap:	1.50 %	Diff.:	-4.79 %
18(C)	Hole:	0.16 %	Electron:	0.79 %	Overlap:	0.35 %	Diff.:	0.63 %
19(C)	Hole:	4.27 %	Electron:	0.65 %	Overlap:	1.66 %	Diff.:	-3.62 %
20(C)	Hole:	1.48 %	Electron:	0.15 %	Overlap:	0.48 %	Diff.:	-1.33 %
21(C)	Hole:	2.12 %	Electron:	0.16 %	Overlap:	0.58 %	Diff.:	-1.96 %
22(C)	Hole:	4.65 %	Electron:	0.72 %	Overlap:	1.83 %	Diff.:	-3.93 %
23(C)	Hole:	0.29 %	Electron:	0.80 %	Overlap:	0.48 %	Diff.:	0.50 %
24(C)	Hole:	6.22 %	Electron:	0.26 %	Overlap:	1.27 %	Diff.:	-5.96 %
25(C)	Hole:	1.06 %	Electron:	0.01 %	Overlap:	0.12 %	Diff.:	-1.04 %
26(C)	Hole:	2.85 %	Electron:	0.37 %	Overlap:	1.03 %	Diff.:	-2.48 %
27(C)	Hole:	0.09 %	Electron:	0.40 %	Overlap:	0.19 %	Diff.:	0.31 %
28(C)	Hole:	3.72 %	Electron:	0.29 %	Overlap:	1.04 %	Diff.:	-3.43 %
29(C)	Hole:	3.57 %	Electron:	0.32 %	Overlap:	1.07 %	Diff.:	-3.25 %
30(C)	Hole:	0.09 %	Electron:	0.46 %	Overlap:	0.21 %	Diff.:	0.37 %
31(C)	Hole:	2.81 %	Electron:	0.30 %	Overlap:	0.91 %	Diff.:	-2.52 %
32(C)	Hole:	0.98 %	Electron:	0.03 %	Overlap:	0.18 %	Diff.:	-0.95 %

Sum of hole shown above: 99.75% Sum of electron shown above: 99.11%

Table S7. The holes and electrons contribution of PymDCz atoms by the multifunctional

wavefunction analyzer.

The number of non-hydrogen atoms: 32

Contribution of each non-hydrogen atom to hole and electron:

1(N)	Hole:	12.32 %	Electron:	18.43 %	Overlap:	15.07 %	Diff.:	6.11 %
2(C)	Hole:	3.79 %	Electron:	29.57 %	Overlap:	10.58 %	Diff.:	25.78 %
3(C)	Hole:	6.67 %	Electron:	1.02 %	Overlap:	2.61 %	Diff.:	-5.65 %
4(C)	Hole:	3.79 %	Electron:	29.57 %	Overlap:	10.58 %	Diff.:	25.78 %
5(N)	Hole:	12.32 %	Electron:	18.43 %	Overlap:	15.07 %	Diff.:	6.11 %
6(C)	Hole:	3.21 %	Electron:	0.98 %	Overlap:	1.77 %	Diff.:	-2.23 %
7(N)	Hole:	6.19 %	Electron:	0.03 %	Overlap:	0.40 %	Diff.:	-6.16 %
8(N)	Hole:	17.39 %	Electron:	0.02 %	Overlap:	0.66 %	Diff.:	-17.37 %
9(C)	Hole:	0.14 %	Electron:	0.03 %	Overlap:	0.06 %	Diff.:	-0.11 %
10(C)	Hole:	0.77 %	Electron:	0.05 %	Overlap:	0.20 %	Diff.:	-0.72 %
11(C)	Hole:	0.77 %	Electron:	0.05 %	Overlap:	0.20 %	Diff.:	-0.72 %
12(C)	Hole:	0.14 %	Electron:	0.03 %	Overlap:	0.06 %	Diff.:	-0.11 %
13(C)	Hole:	0.44 %	Electron:	0.02 %	Overlap:	0.09 %	Diff.:	-0.42 %
14(C)	Hole:	2.54 %	Electron:	0.03 %	Overlap:	0.27 %	Diff.:	-2.51 %
15(C)	Hole:	2.54 %	Electron:	0.03 %	Overlap:	0.27 %	Diff.:	-2.51 %
16(C)	Hole:	0.44 %	Electron:	0.02 %	Overlap:	0.09 %	Diff.:	-0.42 %
17(C)	Hole:	1.64 %	Electron:	0.02 %	Overlap:	0.18 %	Diff.:	-1.62 %
18(C)	Hole:	0.05 %	Electron:	0.00 %	Overlap:	0.01 %	Diff.:	-0.04 %
19(C)	Hole:	1.09 %	Electron:	0.03 %	Overlap:	0.20 %	Diff.:	-1.06 %
20(C)	Hole:	0.29 %	Electron:	0.00 %	Overlap:	0.02 %	Diff.:	-0.29 %
21(C)	Hole:	0.30 %	Electron:	0.00 %	Overlap:	0.02 %	Diff.:	-0.29 %
22(C)	Hole:	1.09 %	Electron:	0.03 %	Overlap:	0.20 %	Diff.:	-1.06 %
23(C)	Hole:	0.05 %	Electron:	0.00 %	Overlap:	0.01 %	Diff.:	-0.04 %
24(C)	Hole:	1.64 %	Electron:	0.02 %	Overlap:	0.18 %	Diff.:	-1.62 %
25(C)	Hole:	1.09 %	Electron:	0.01 %	Overlap:	0.12 %	Diff.:	-1.08 %
26(C)	Hole:	3.65 %	Electron:	0.01 %	Overlap:	0.14 %	Diff.:	-3.65 %
27(C)	Hole:	0.17 %	Electron:	0.05 %	Overlap:	0.09 %	Diff.:	-0.12 %
28(C)	Hole:	4.50 %	Electron:	0.28 %	Overlap:	1.11 %	Diff.:	-4.23 %
29(C)	Hole:	4.50 %	Electron:	0.28 %	Overlap:	1.11 %	Diff.:	-4.23 %
30(C)	Hole:	0.17 %	Electron:	0.05 %	Overlap:	0.09 %	Diff.:	-0.12 %
31(C)	Hole:	3.65 %	Electron:	0.01 %	Overlap:	0.14 %	Diff.:	-3.65 %
32(C)	Hole:	1.09 %	Electron:	0.01 %	Overlap:	0.12 %	Diff.:	-1.08 %

Sum of hole shown above: 98.42% Sum of electron shown above: 99.10%

5. NMR Spectra of Monomers and C-3 Selenocyanation Products

^{1}H NMR (400 MHz, $CDCl_3$)

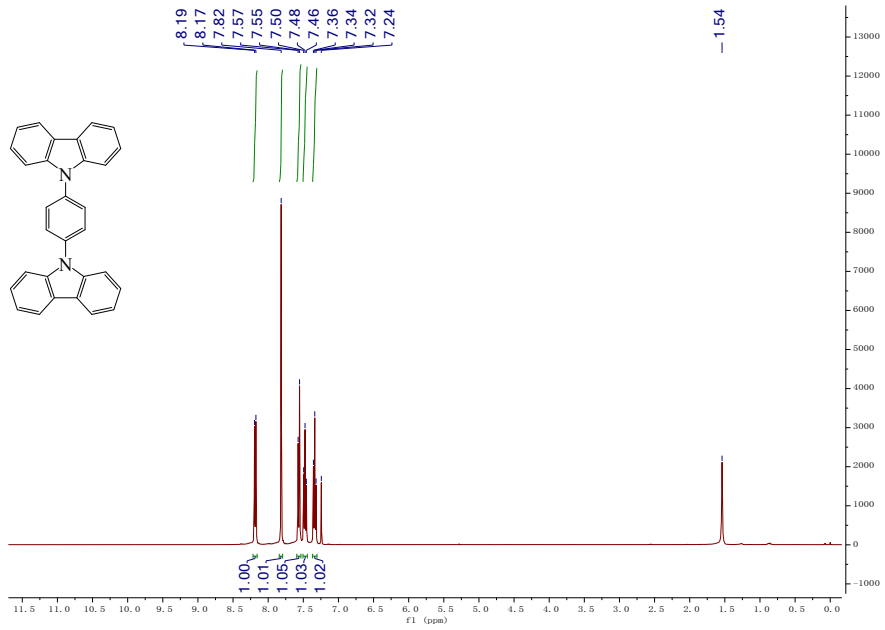

^{13}C NMR (100 MHz, $CDCl_3$)

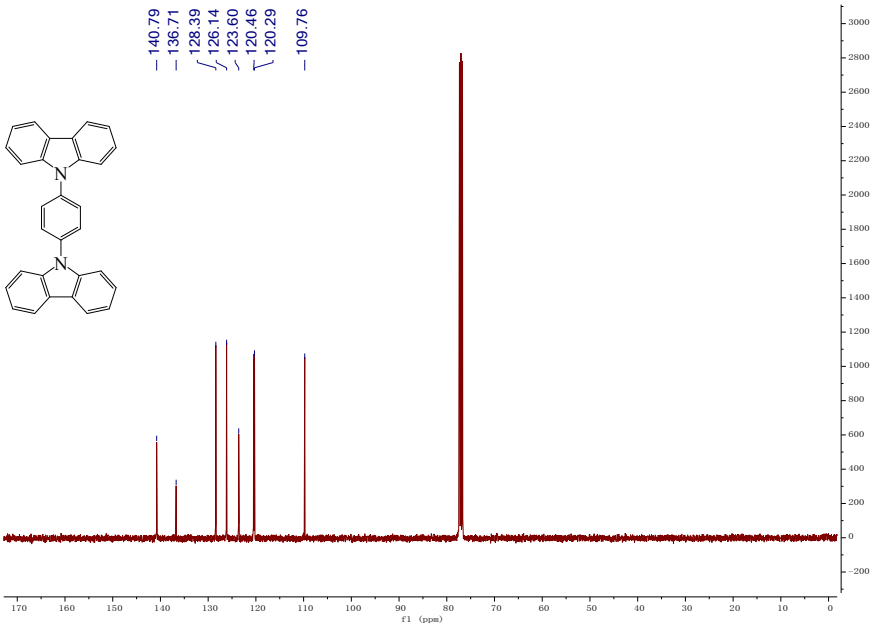

^{1}H NMR (400 MHz, $CDCl_3$)

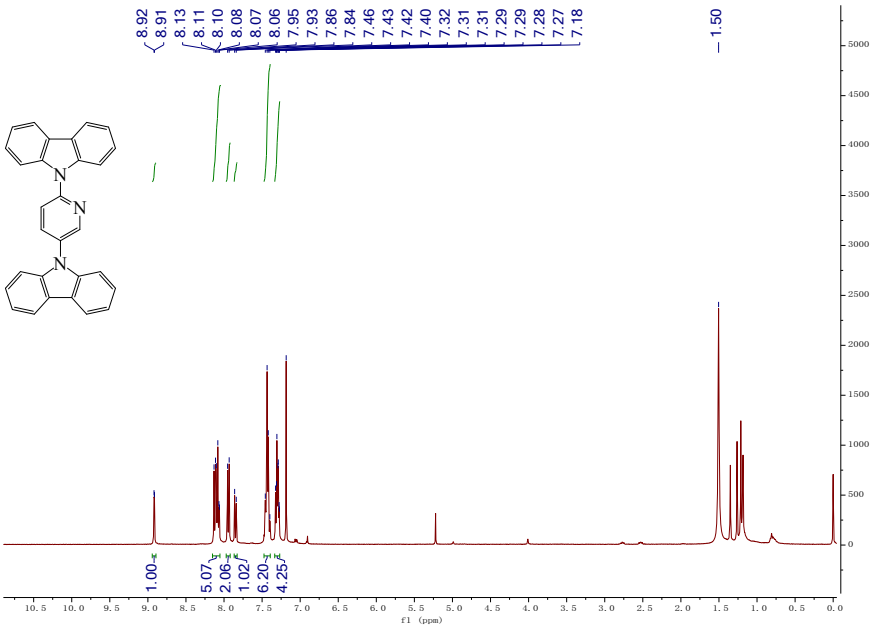

^{13}C NMR (100 MHz, $CDCl_3$)

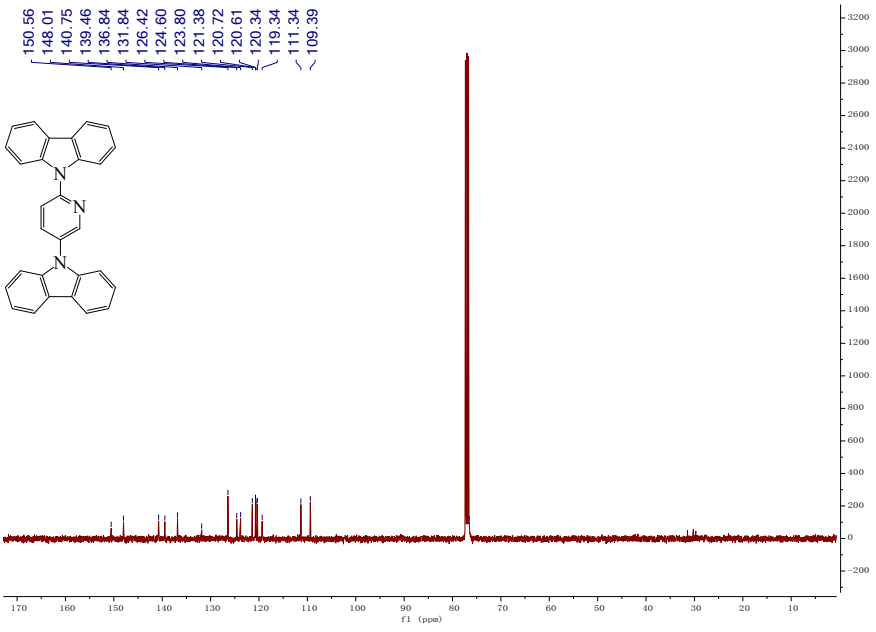

^{1}H NMR (400 MHz, $CDCl_3$)

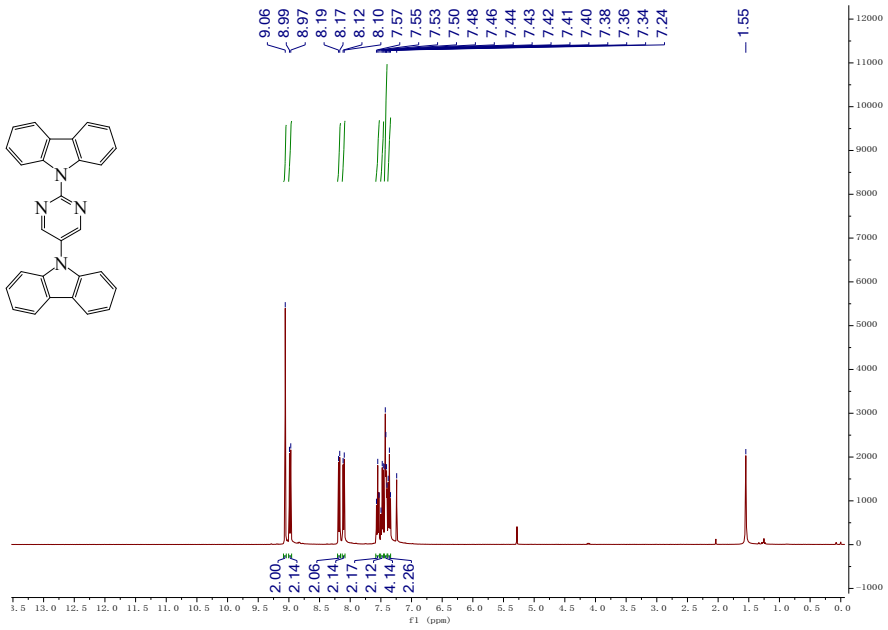

^{13}C NMR (100 MHz, $CDCl_3$)

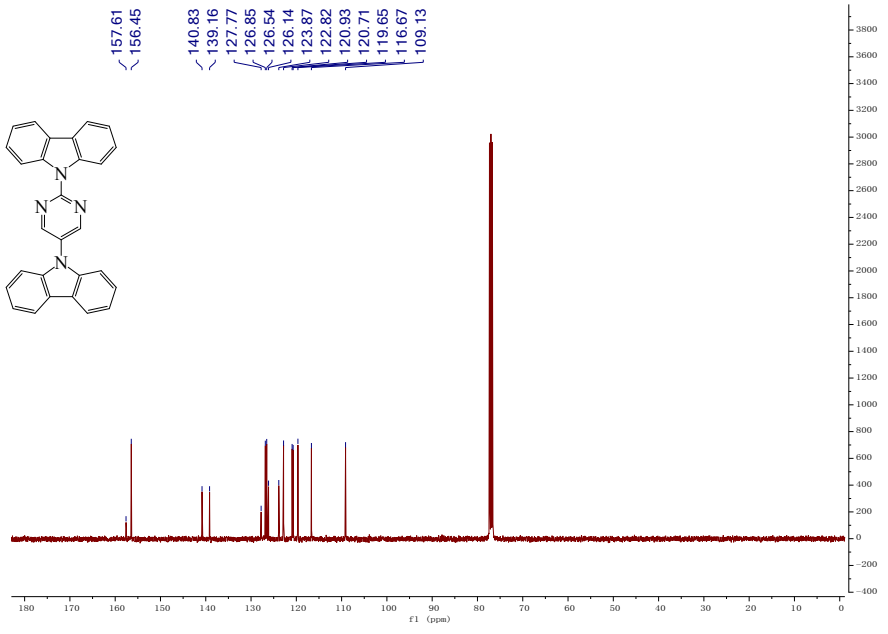

^{1}H NMR (400 MHz, DMSO-*d6*)

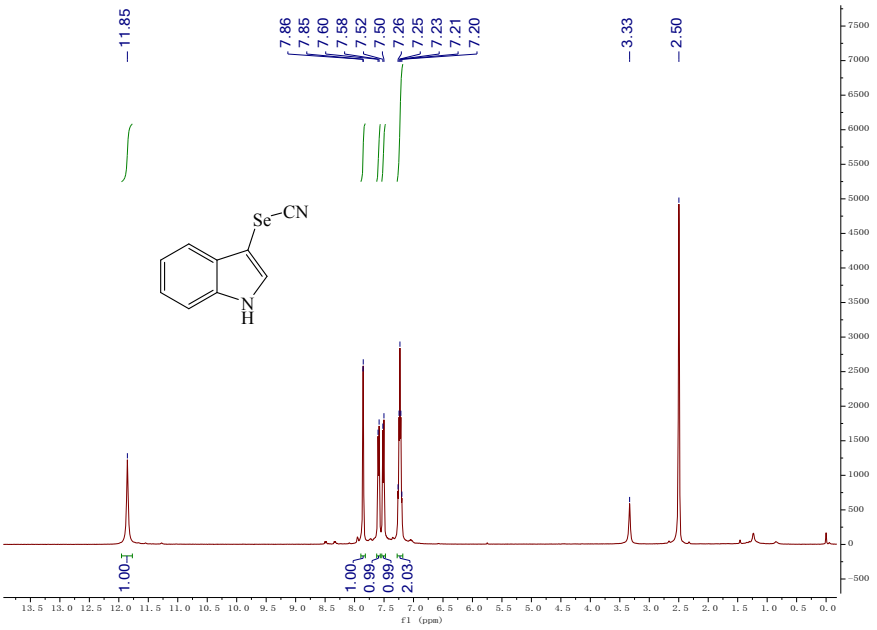

^{13}C NMR (100 MHz, DMSO-*d6*)

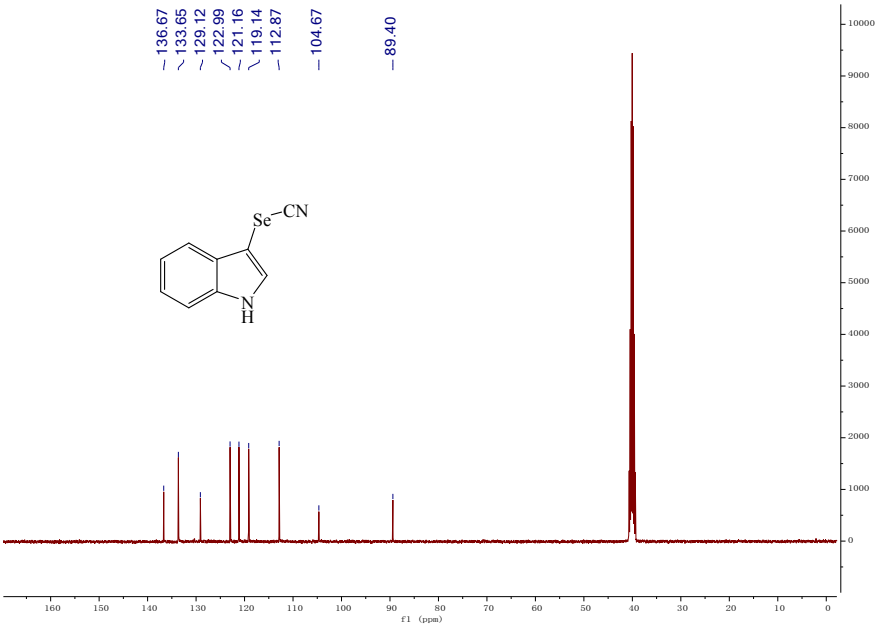

^{1}H NMR (400 MHz, DMSO-*d6*)

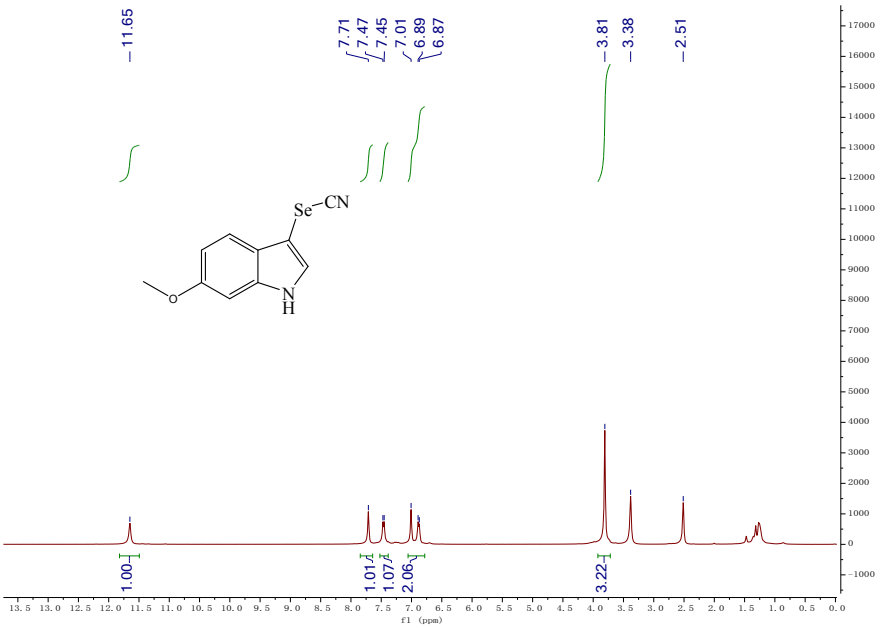

^{13}C NMR (100 MHz, DMSO-*d6*)

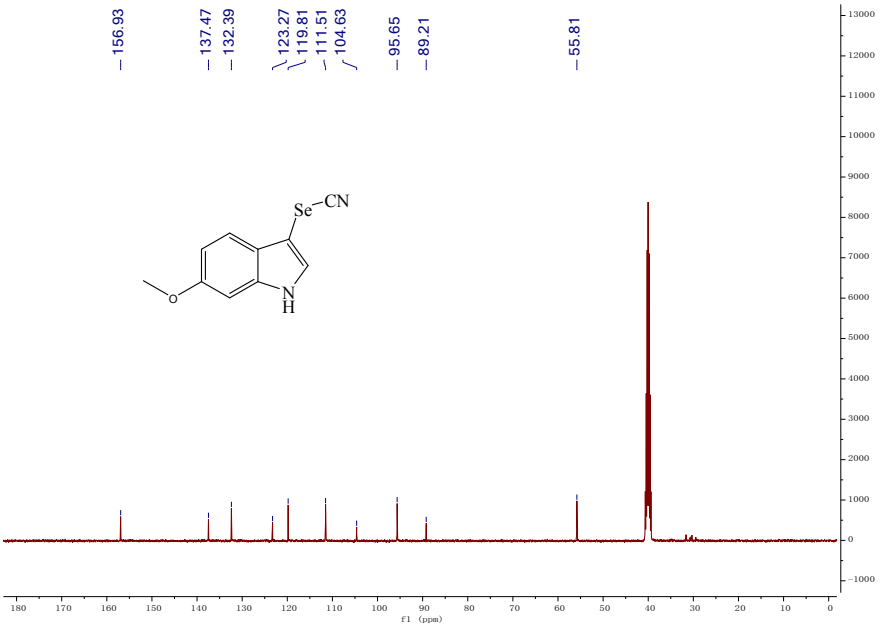

^{1}H NMR (400 MHz, $CDCl_3$)

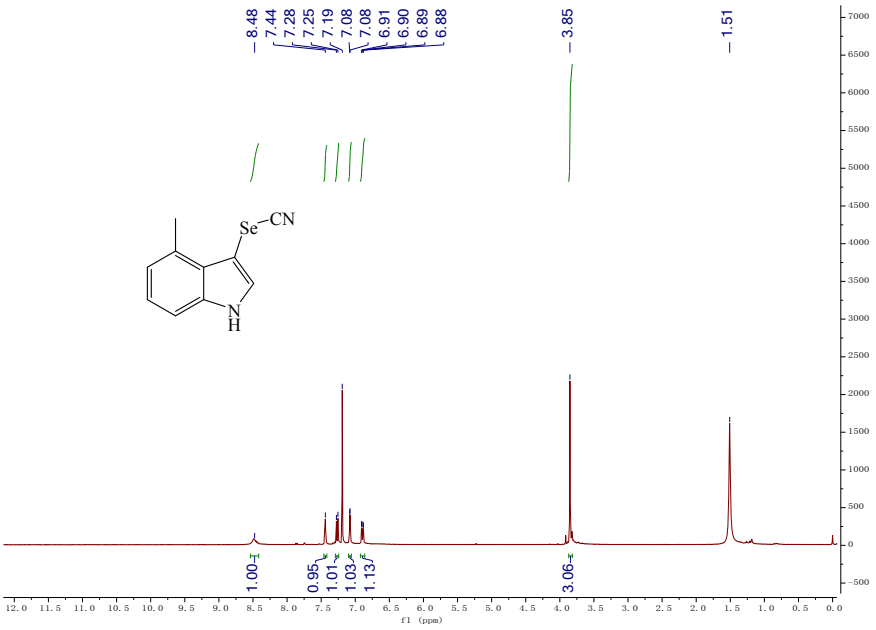

^{13}C NMR (100 MHz, $CDCl_3$)

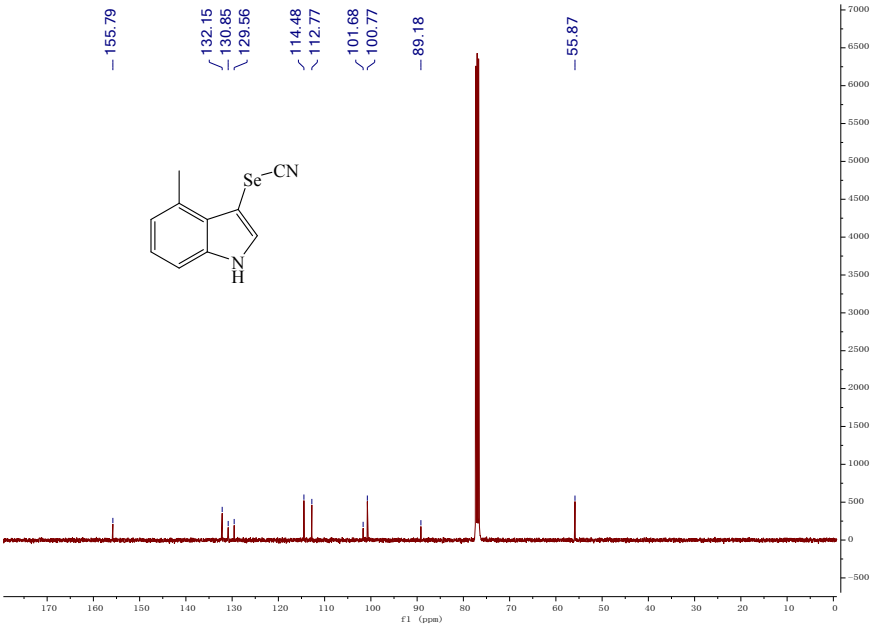

^{1}H NMR (400 MHz, DMSO-*d6*)

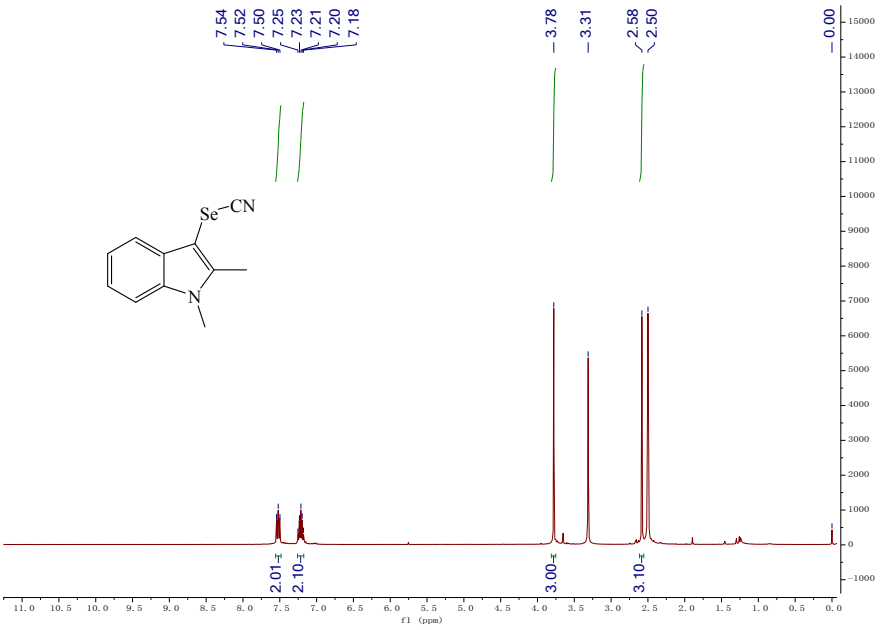

^{13}C NMR (100 MHz, DMSO-*d6*)

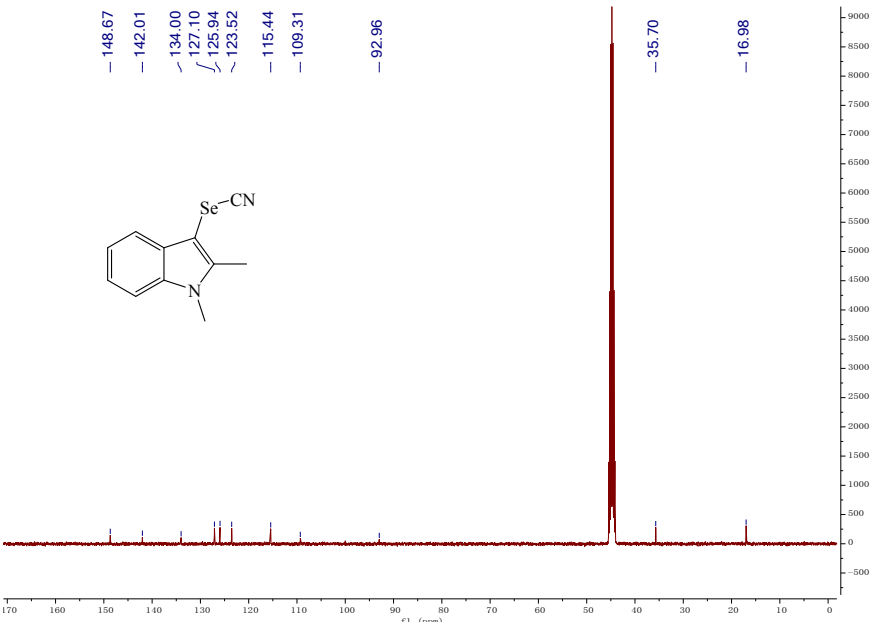

^{1}H NMR (400 MHz, DMSO-*d6*)

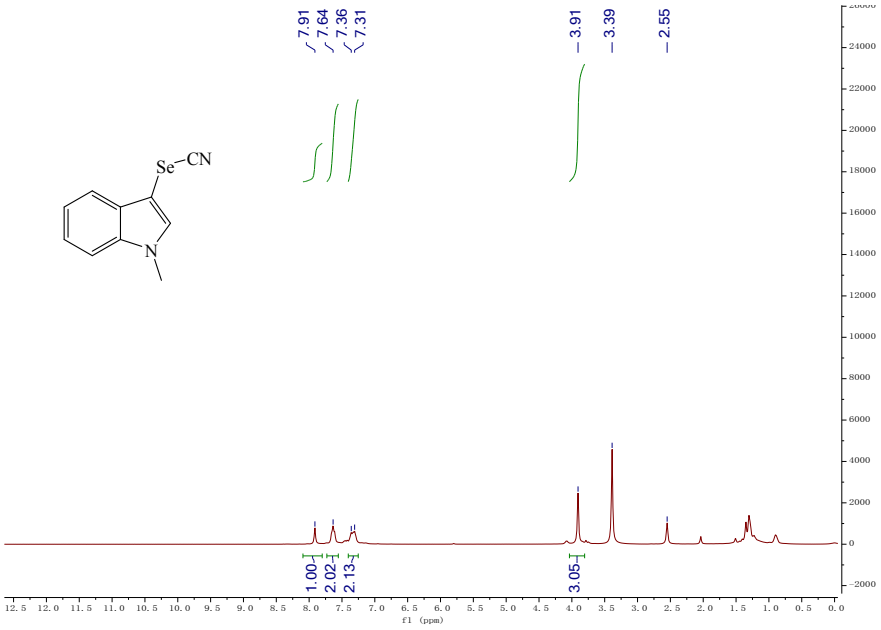

^{13}C NMR (100 MHz, DMSO-*d6*)

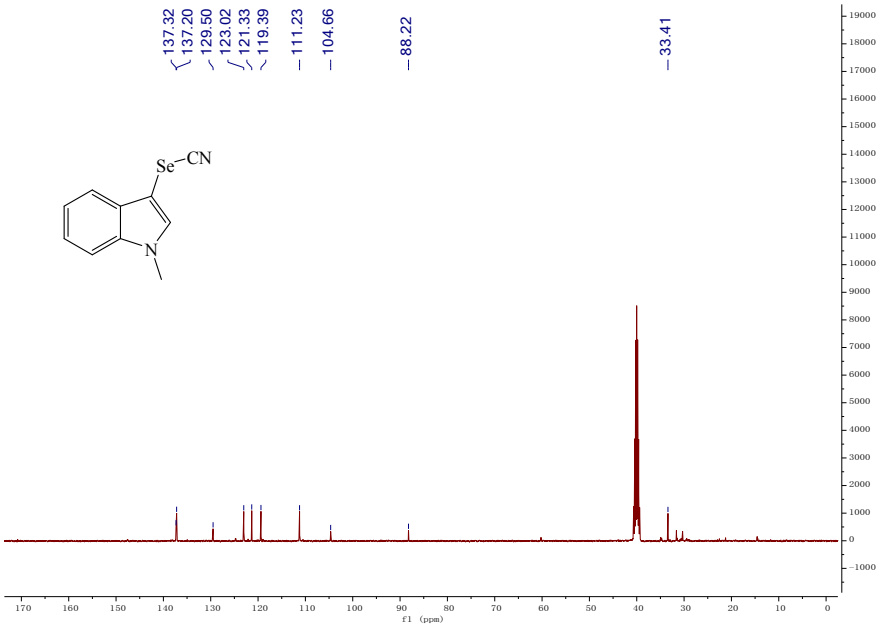

^{1}H NMR (400 MHz, $CDCl_3$)

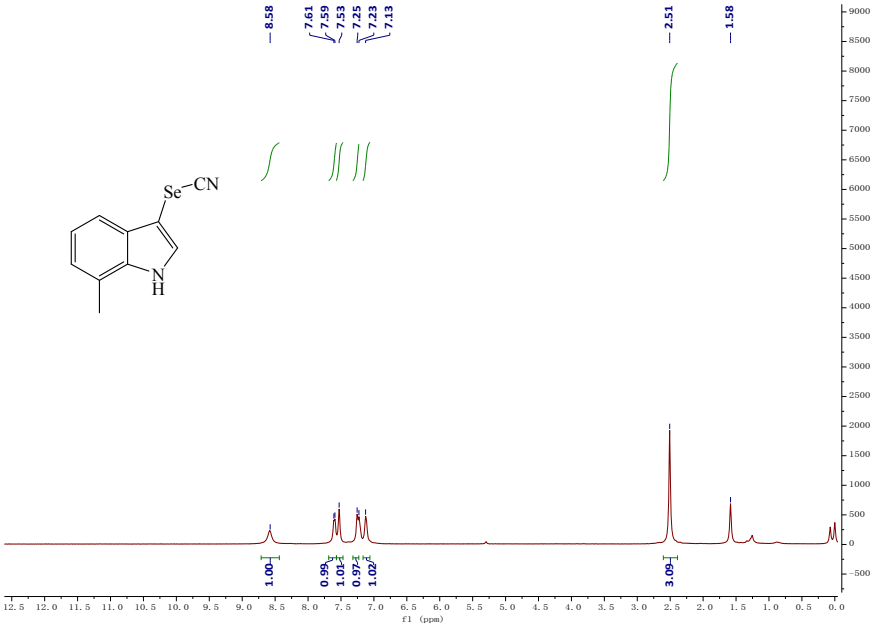

^{13}C NMR (100 MHz, $CDCl_3$)

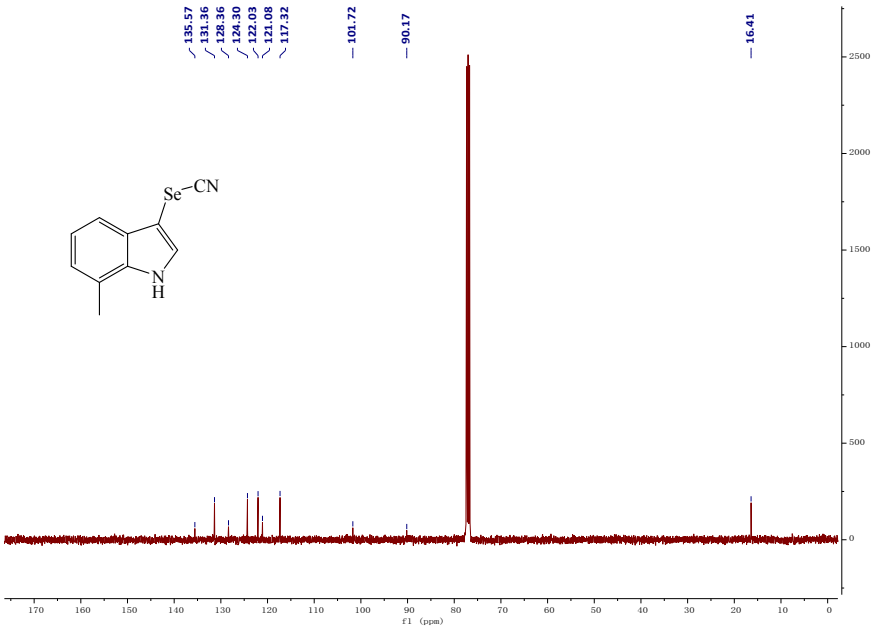

^{1}H NMR (400 MHz, $CDCl_3$)

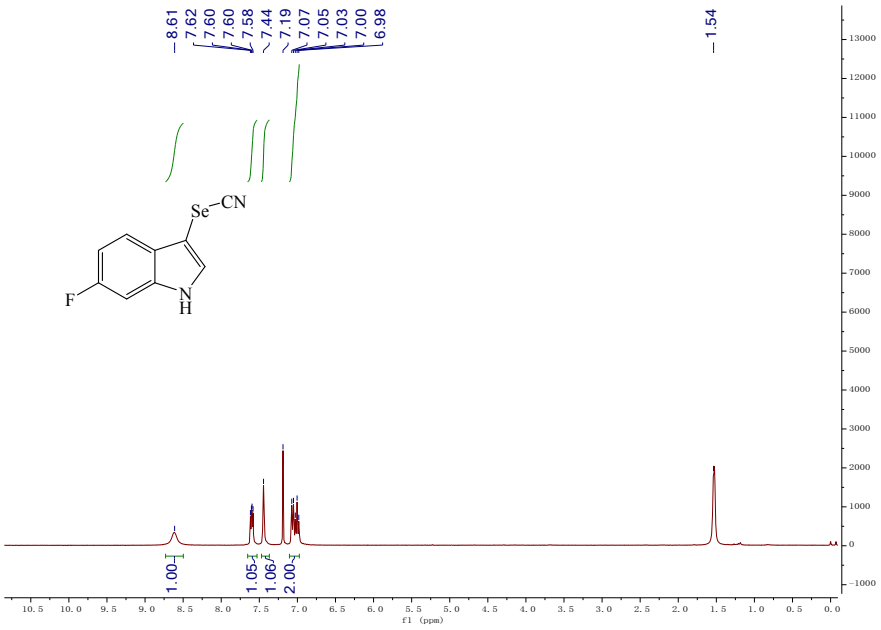

^{13}C NMR (100 MHz, $CDCl_3$)

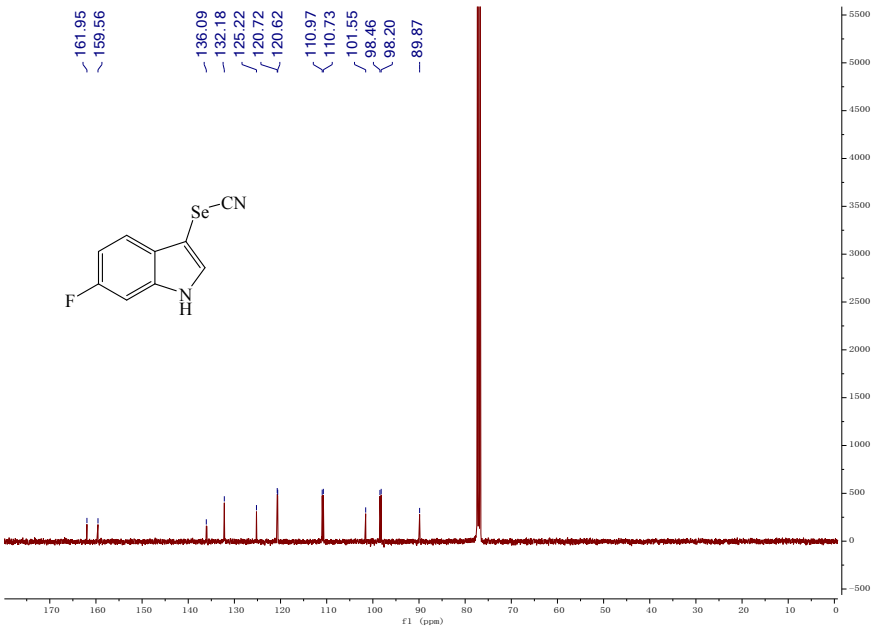

^{1}H NMR (400 MHz, $CDCl_3$)

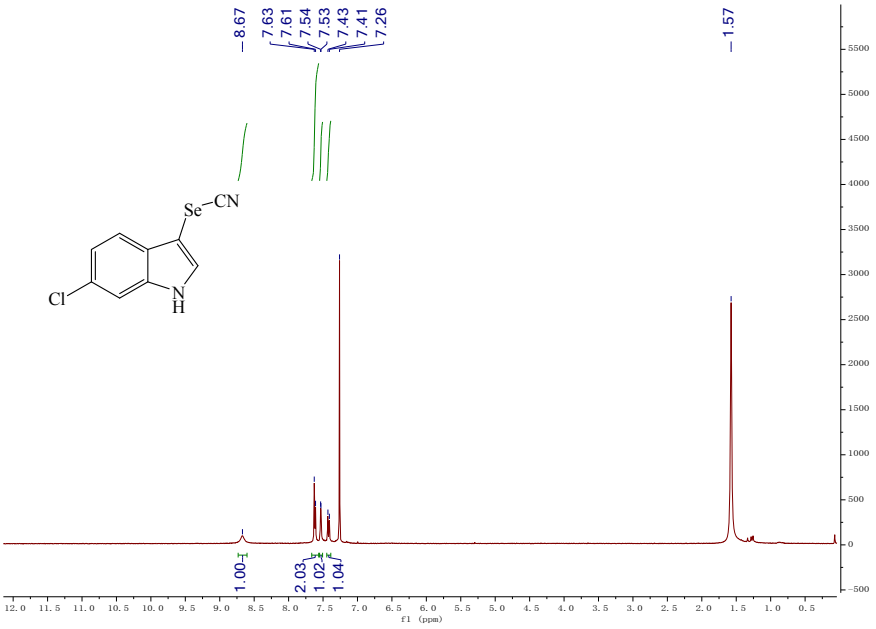

^{13}C NMR (100 MHz, $CDCl_3$)

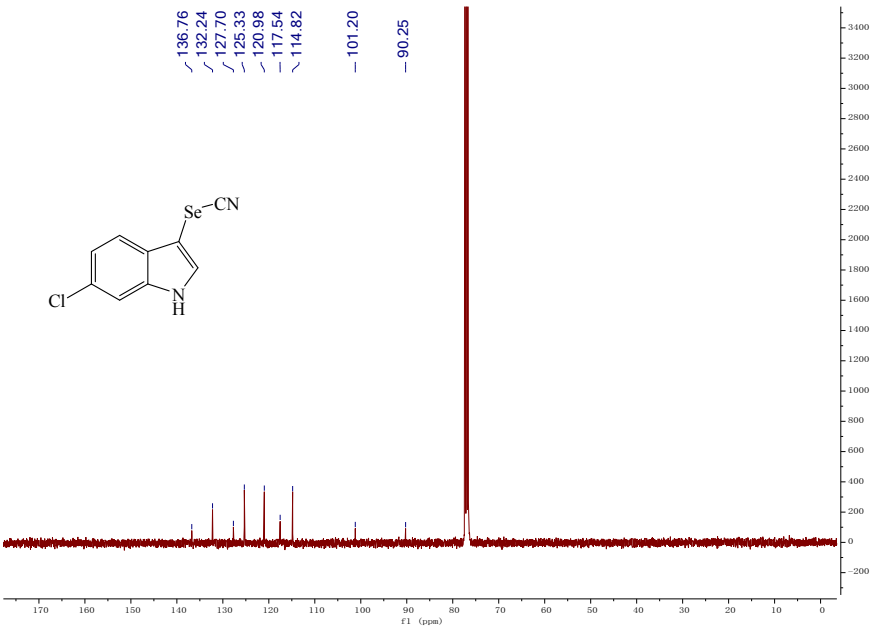

^{1}H NMR (400 MHz, $CDCl_3$)

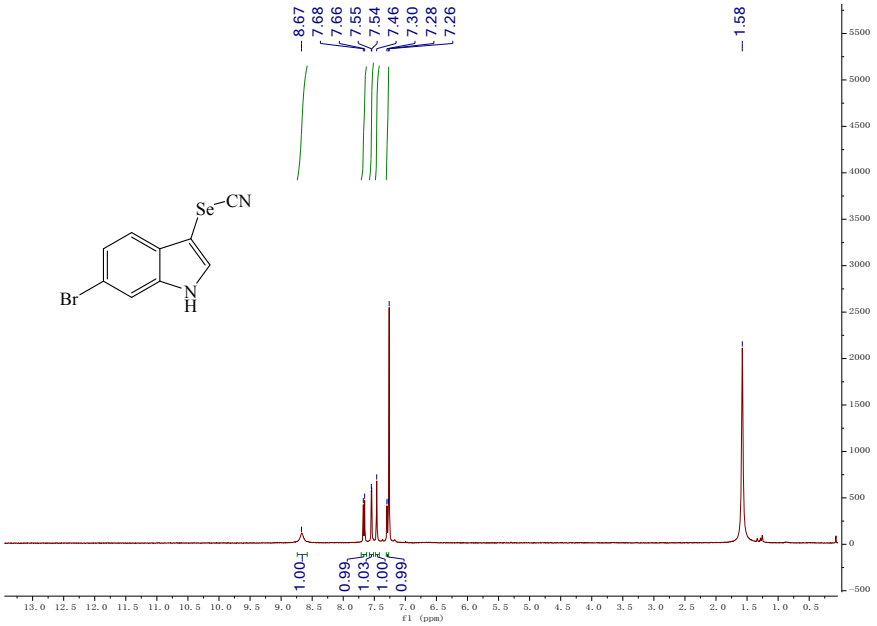

^{13}C NMR (100 MHz, $CDCl_3$)

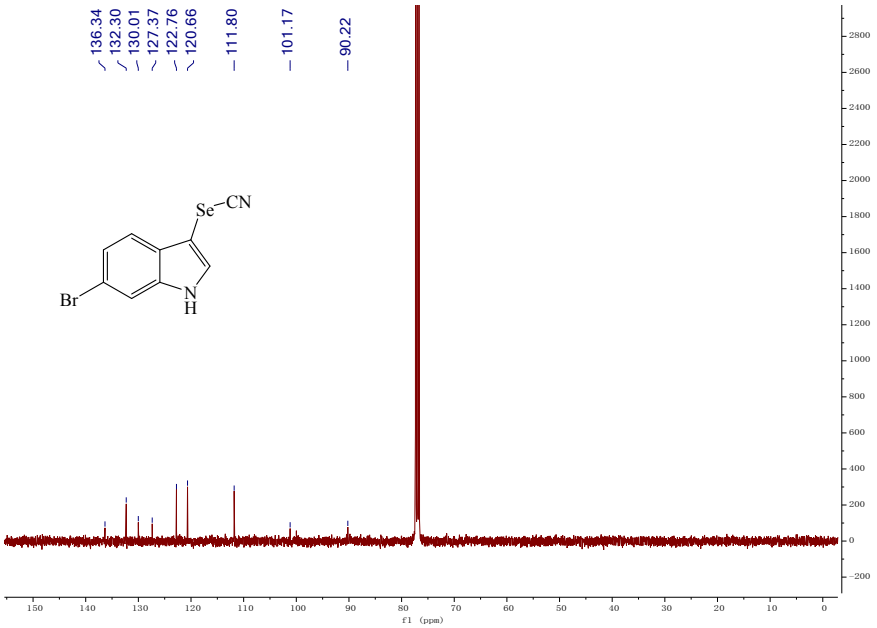

^{1}H NMR (400 MHz, $CDCl_3$)

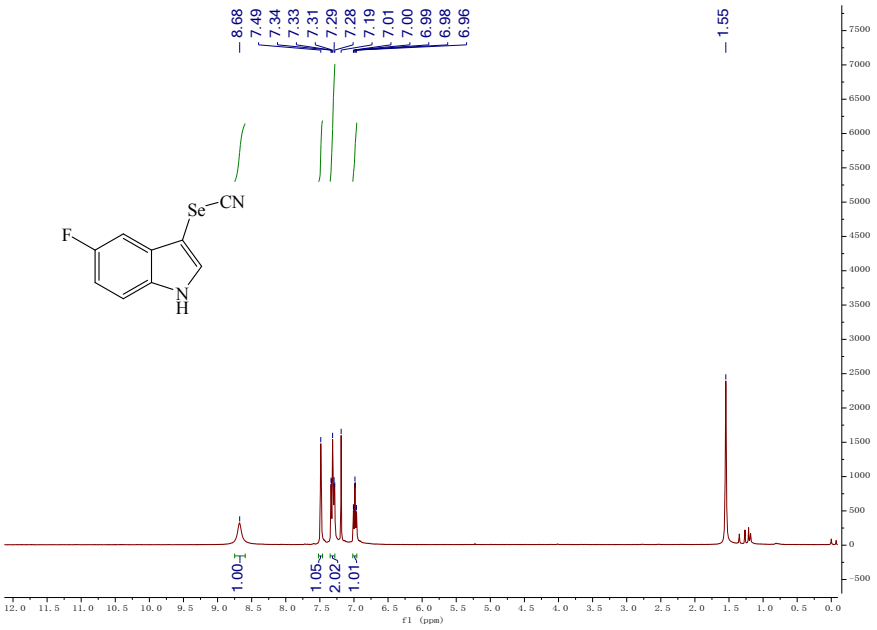

^{13}C NMR (100 MHz, $CDCl_3$)

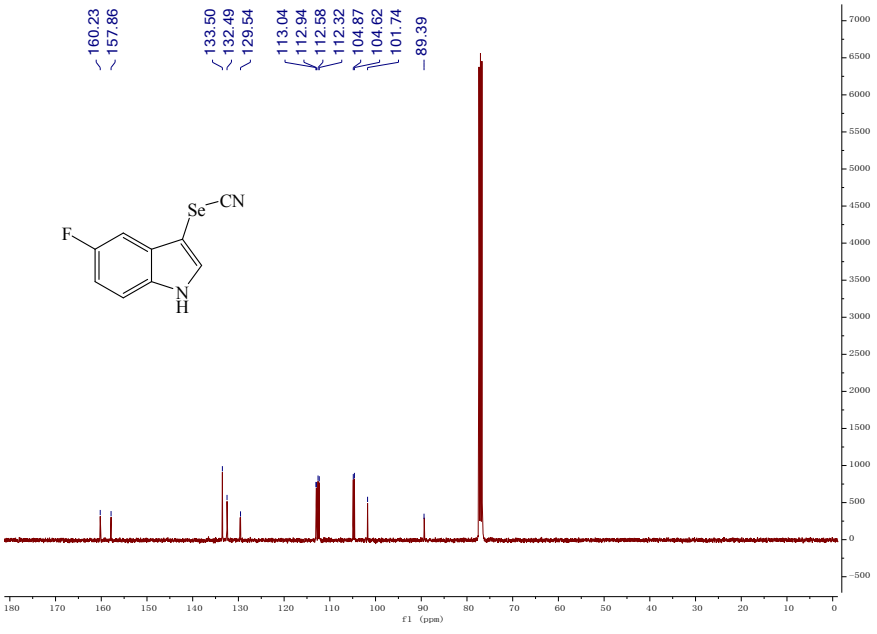

^{1}H NMR (400 MHz, $CDCl_3$)

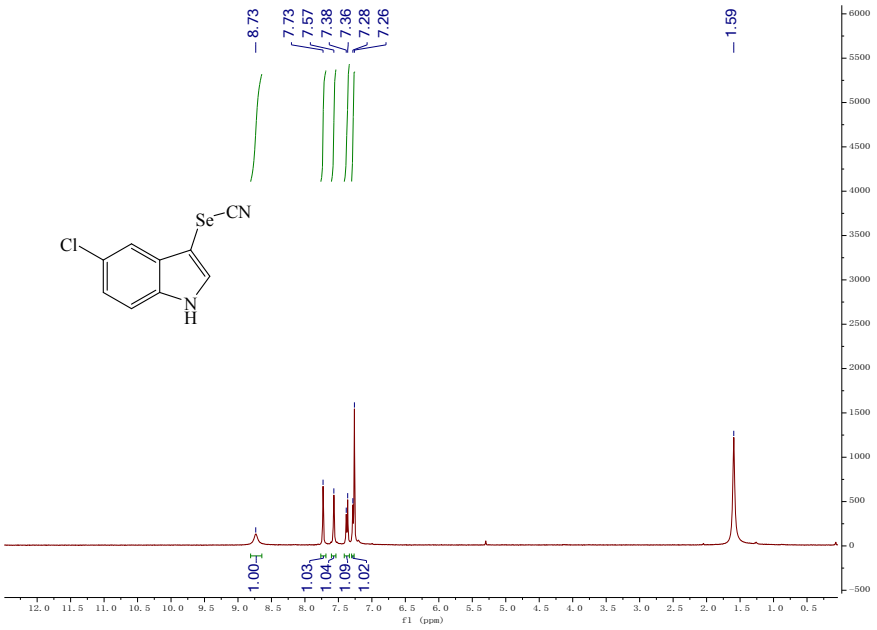

^{13}C NMR (100 MHz, $CDCl_3$)

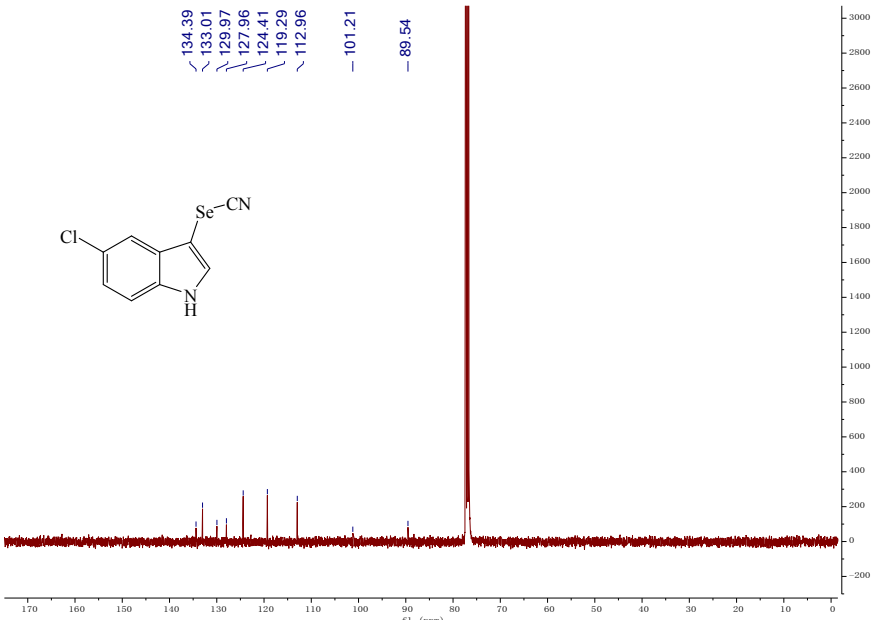

^{1}H NMR (400 MHz, $CDCl_3$)

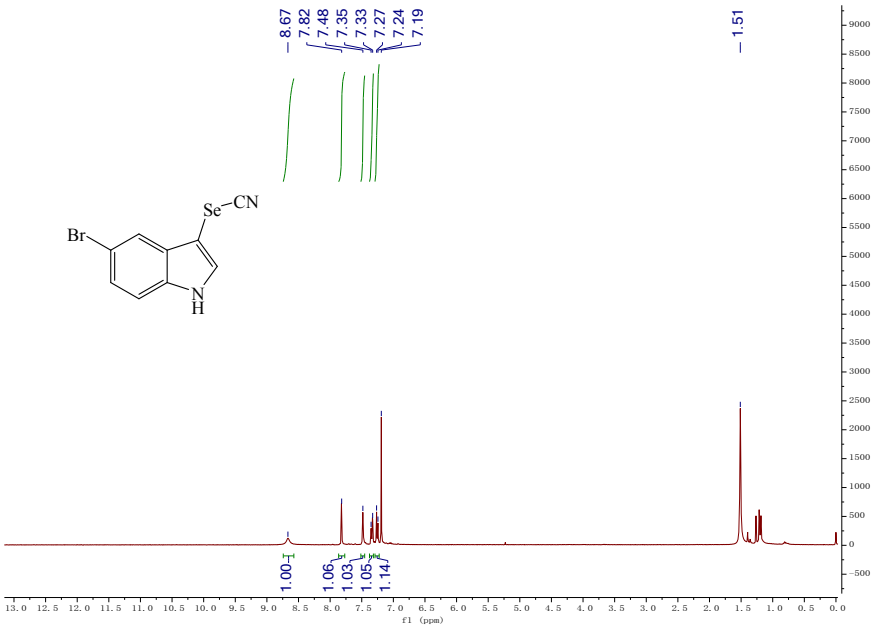

^{13}C NMR (100 MHz, $CDCl_3$)

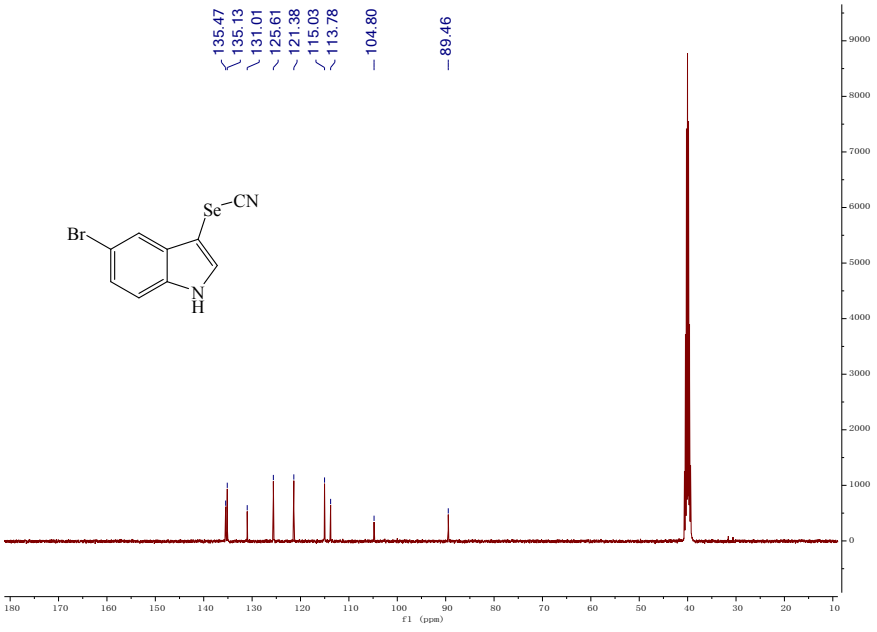

^{1}H NMR (400 MHz, DMSO-*d6*)

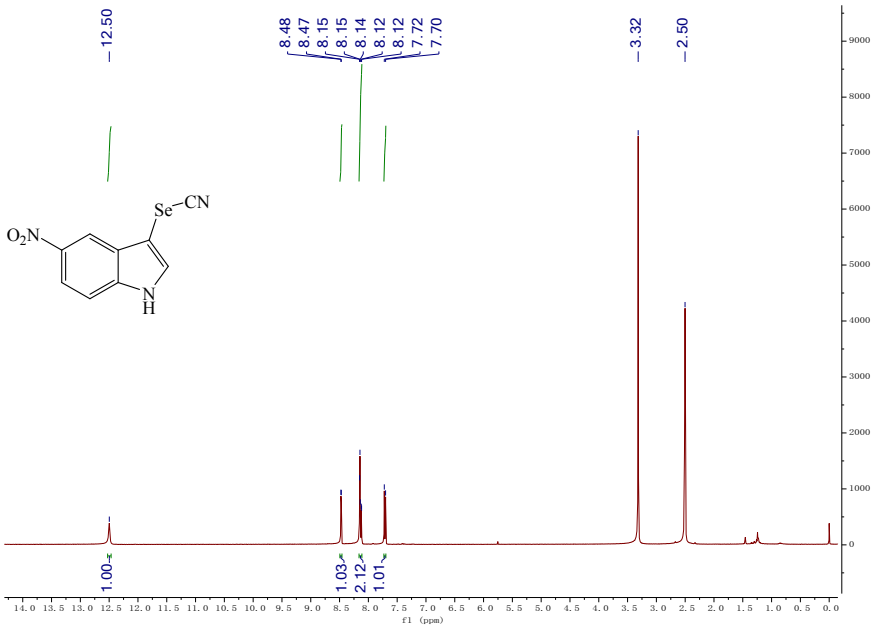

^{13}C NMR (100 MHz, DMSO-*d6*)

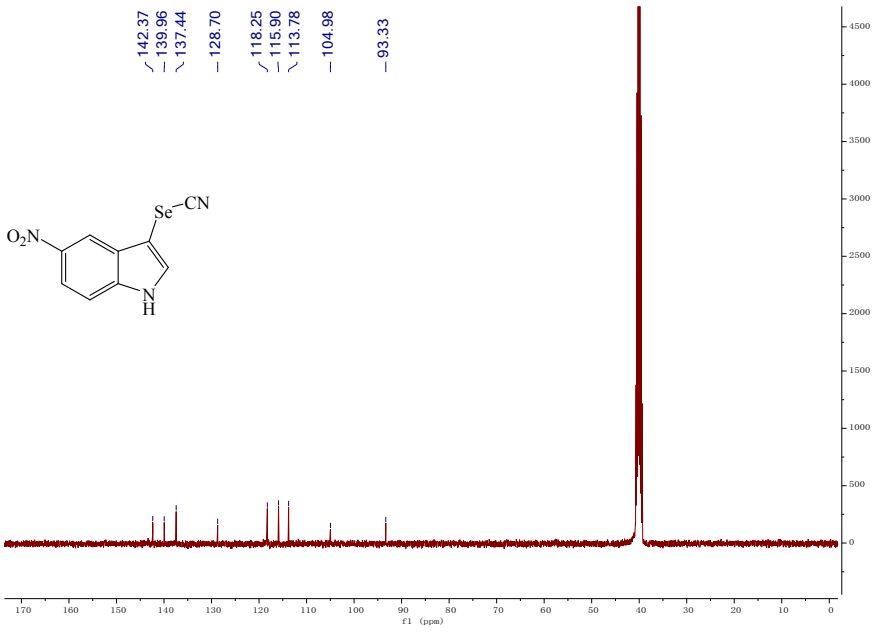

^{1}H NMR (400 MHz, DMSO-*d6*)

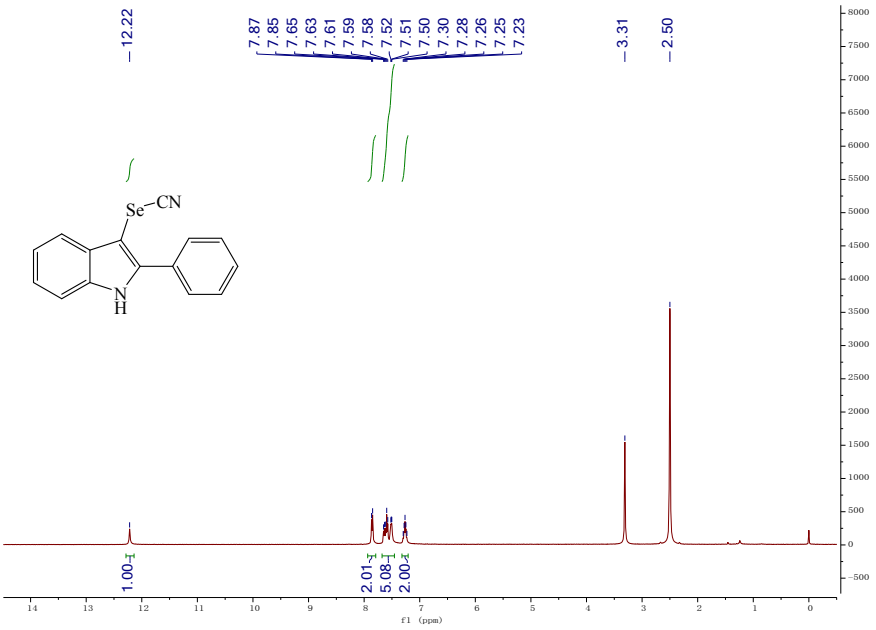

^{13}C NMR (100 MHz, DMSO-*d6*)

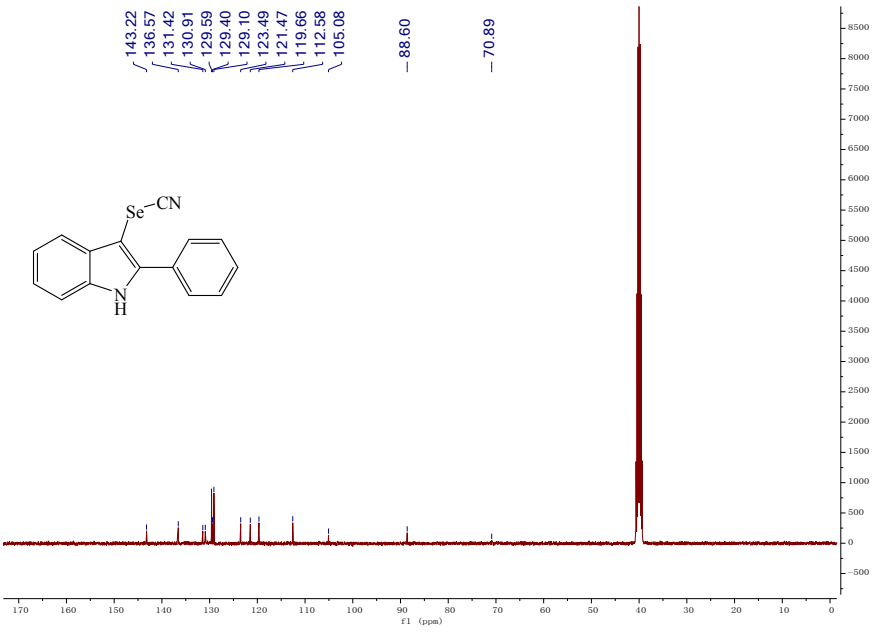

6. Supplementary References

1 S. Zhang, R. Chen, J. Yin, F. Liu, H. Jiang, N. Shi, Z. An, C. Ma, B. Liu and W. Huang, 2010, 2008-2011.

2 T. Lu and F. Chen, J. Comput. Chem., 2012, 33, 580–592.